TABLE OF CONTENTS

Technical Papers on Gas Technology

International Conference on Petroleum Engineering 2016 (ICPE-2016)
Bangladesh University of Engineering & Technology (BUET)
Dhaka-1000, Bangladesh

ICPE (2016-017)

Future Prospect Analysis of Liquefied Petroleum Gas (LPG) and Liquefied Natural Gas (LNG) in Bangladesh: Economic and Technological Case Studies

Md. Shaheen Shah[1]*, Md. Shimul Hossain[1], Farzana Yeasmin Nipa[1], Simanto Kumar Pal[1], Md. Rashidul Islam[1], S.M. Samiur Sany[1]

[1]Department. of Petroleum and Mining Engineering, Jessore University of Science and Technology, Jessore-7408, Bangladesh

ABSTRACT

Bangladesh is one of the densely populated countries in the world. The energy consumer is increasing gradually in the country. The key energy source in the country is natural gas but the supply is less than the demand. The annual gas consumption is about 1 Tcf per year and it is expected that the gas demand will be approximately 58.2 Tcf at the end of 2050.The country is facing gas crisis right now. The pipeline supply is not accessible in all of the part of the country. Liquefied Natural Gas (LNG) and Liquefied Petroleum Gas (LPG) can be a solution for this problem. The LPG demand is increasing sharply because of its very clean burning, cost effectiveness, easy transportation facilities. Currently, the LPG demand in Bangladesh is almost 100,000 mt per year. Kailashtila, Sylhet and Chittagong LPG plants are supplying roughly 15-20 percent of the current demand and private players import the remaining 80 percent. The price of LPG has dropped by more than 50 percent in the international market although the price does not match in Bangladesh with the world market yet. On the other hand, the price of natural gas in the country has increased by 26.29 percent on an average, with a hike of 50 percent for domestic users. LNG can be imported to decrease the pipe line gas crisis. Bangladesh is proceeding with a plan for setting up 3.5 million tons per year LNG import facility at Matarbari in Maheshkhali Island to Chittagong city. It requires 600 times less space than natural gas and neither corrosive nor toxic for LNG. It is estimated that about 4 million ton of LNG would be required annually in the country. The government of Bangladesh should be more positive to introduce LPG and LNG for developing all the part of the country.

Keywords: LPG, LNG, Cost Effectiveness, Transportation Facilities, Bangladesh.

*Corresponding Author address
Email: shaheenshah_just@yahoo.com

1. INTRODUCTION

Natural gas is the main energy source in Bangladesh. It has been the life line of the commercial energy source of Bangladesh for several decades (Fig.1). In 2010 natural gas share in power generation in the country was about 88%. The annual gas consumption is 1 Tcf per year and the estimate gas reserve has been 16 Tcf as of December 2011[17]. Gas demand in Bangladesh is increasing day by day. At the end of 2050, the gas demand will be 58.2 Tcf (Table.1)[33].

Table.1: Long term overview of gas demand in Bangladesh [16].

Sector Wise	2011-2050 year (Tcf)
Power	37.3
Fertilizer	3.8
Residential/Commercial/Other	4.4
Industrial	12.7
Total	58.2

With the demand of gas, the price of gas also increased by 26.29 percent on an average, with a hike of 50 percent for domestic users. Domestic users will now have to shell out Bangladesh Taka (BDT) 600 and BDT 650 for single and double burners respectively, up from BDT 400 and BDT 450 respectively. Metered connections will see a hike to BDT 7 per cubic foot from BDT 5.16 [13].

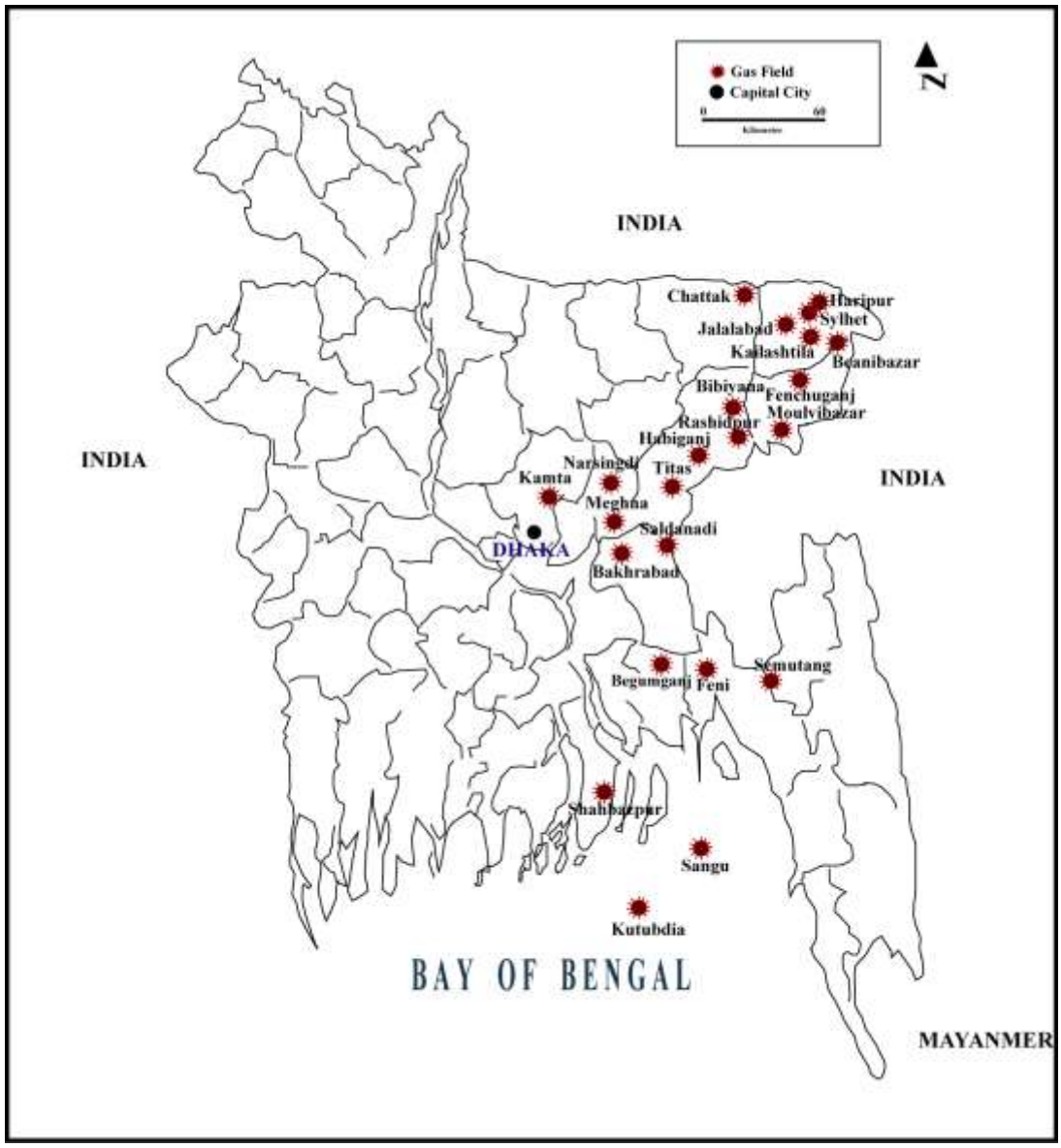

Fig. 1: Gas Fields in Bangladesh [Modified after 17,33]

Otherwise, LPG prices have dropped by more than 50 percent in the international market since, February 2014. The price per metric tons of LPG was USD 1,400 in December 2013, but has dropped to USD 550 in April 2016 [22]. LPG made up chiefly of propane or butane, is a by-product of gasoline and diesel fuel refining. LPG changes to the liquid state at the moderately high pressures found in an LPG vehicle's fuel tank. LPG is formed naturally, interspersed with deposits of petroleum and natural gas.

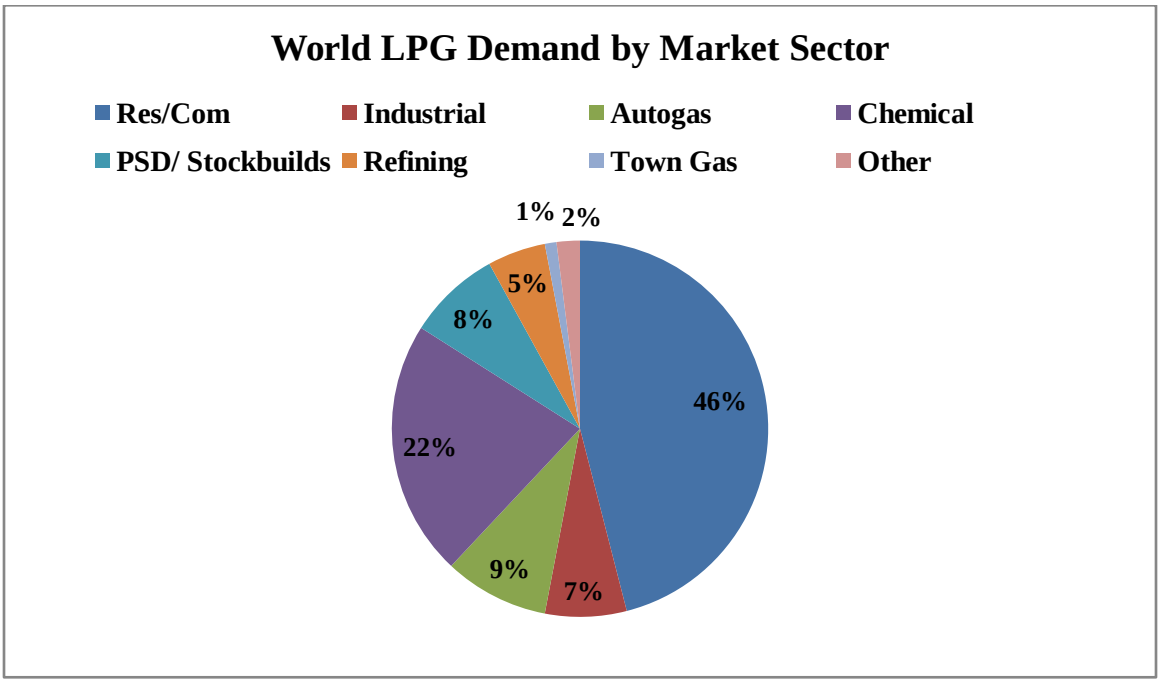

Fig. 2: World LPG demand by market sector [44]: Abbreviations, PSD= Price Sensitive Demand; Res= Residential; Com= Commercial.

LPG demand increasing in Bangladesh day by day although the price does not matching yet with world market. LPG demand in Bangladesh is 100,000 mt/year [17]. The Government LP Company on an average has been supplying over 20,000 Metric tons (M.tons) of LPG to various parts of the country which is roughly 15%-20% of the current demand and private players import the remaining 80 percent [7]. LPG is using in present world mostly in residential and commercial purpose. Besides, it is using also as the purpose of town gas, industrial, chemical, refining, price sensitive demand (Fig.2) [44].

With the decreasing natural gas supply, pipeline gas demand increase. For natural gas crisis, many industry lost huge amount every year. For this reason, LNG can be a solve way. Bangladesh government already adopted a plan for importing LNG from Maheshkhali to Chittagong city ring main gas network. LNG is a natural product occurring in underground deposits [2,6,33]. In terms of composition, it is more than 90 percent methane (CH_4). Natural gas retains its gaseous form down to a temperature of minus 162 degrees Celsius. Below this point it becomes a liquid and occupies a far smaller volume. LNG is about 1/600th the volume of natural gas at standard temperature and pressure (STP) that means it requires 600 times less space than natural gas. It's a clear, colorless, odorless liquid. LNG is neither corrosive nor toxic and weighs less than half the weight of water. It is not explosive. Hence, it can be a good result [1,14,23,36].

2. NATURAL GAS OVERVIEW IN BANGLADESH

Natural gas has played a vital role in the development of both the power and fertilizer sectors in Bangladesh and the major indigenous source of energy in Bangladesh and accounts for almost one-half of all primary energy used in the country. Natural gas of Bangladesh is very pure, with about 95% to 99% methane and almost no sulphur (Table.2) [17,38].

Table.2: Composition of Natural Gas in Bangladesh [17,25,35,38].

Composition	Amount %
Methane	97.33
Ethane	1.72
Propane	0.35
Higher Hydrocarbons	0.19

The current total gas reserves of 16.36 Tcf its 16.02 Tcf is in 24 onshore gas fields [45]. Gas supplies meet 56% of domestic energy demand. The country has an average daily natural gas production of around 2,700 million cubic feet, a supply that is insufficient to meet its demand of more than 3,200 MMcf/d [8,33]. Natural gas is covering about 49.2% primary energy source in the Bangladesh (Fig.3).

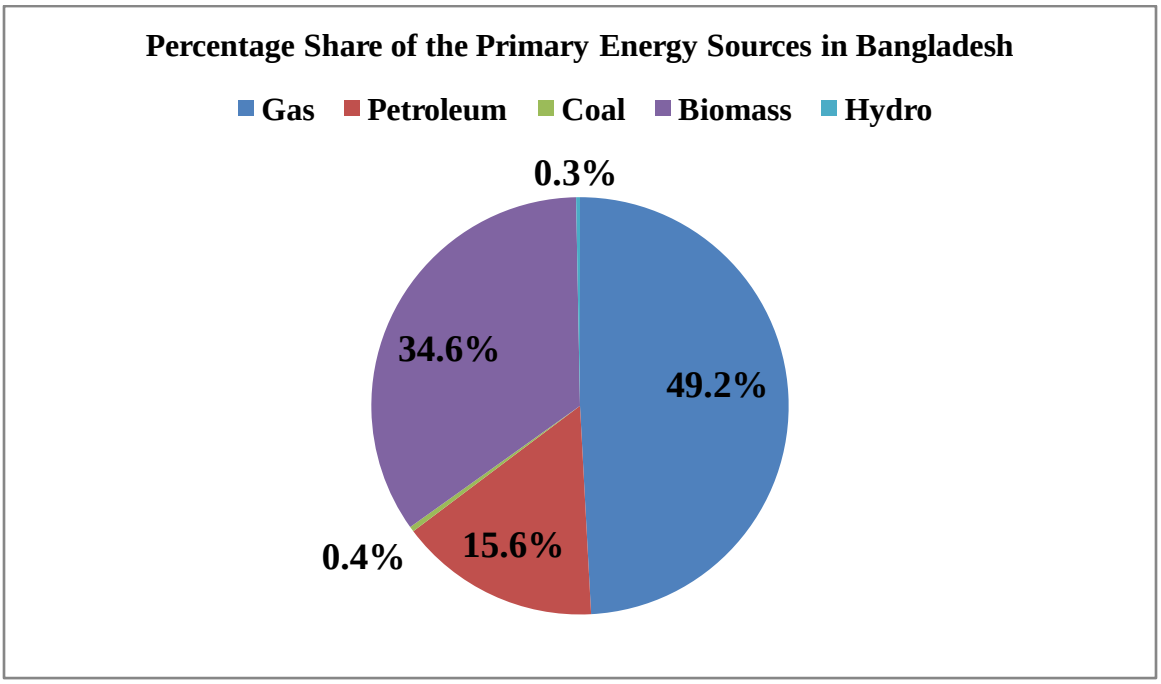

Fig.3: Percentage share of the primary energy sources in Bangladesh [27,40].

There are currently no exports or imports of natural gas, so the growth of domestic consumption tracks the growth of domestic production, demonstrating an overall growth rate of 7 percent per year over the last several decades [8,9]. Since, natural gas is the only indigenous source of commercial energy in the country (ignoring little coal deposits), it is important to understand how natural gas demand will evolve in future in response to and in spurring the rapid economic growth [42].

3. LPG AND LNG PROCESS

LPG is made during natural gas processing and oil refining. From associated gas it compressed and then cooled with refrigeration (Fig.4). It stored pressurized as a liquid in cylinders or tanks. This LPG can be

used as is or separated into its three primary parts: propane, butane and isobutene. About 60% is produced from the natural gas and other 40% is produced during the crude oil refining process [15].

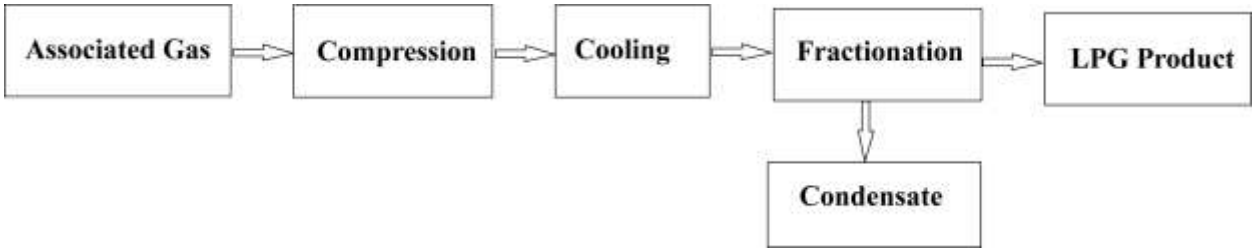

Fig.4: Flow diagram of LPG product production from associated gas [Modified after 1,24,41].

Natural gas (NG) can be converted to LNG by cooled down temperature. It can be Single Flow (for less than 0.2 mtpa LNG) or Mixed Fluid Cascade (for 3 to 10 mtpa LNG) process [37,41].A plate-fin heat exchanger set in a cold box, where the NG gas is cooled-down to LNG temperatures by a two stage single MR (Mixed Refrigerant) cycle. A separation vessel, where the mixed refrigerant (MR) is separated in a liquid fraction, and which provides the cold temperature after expansion in a J-T (Joule-Thompson) valve for the NG pre-cooling and liquefaction. The gas from the separator provides the LNG sub-cooling temperature after J-T expansion at the bottom of the heat exchanger. The cycle gas streams leaving the heat exchanger are recompressed in the two stage turbo compressor. The compressed cycle gas is cooled and partly condensed against air or water (Fig.5) [14,21].

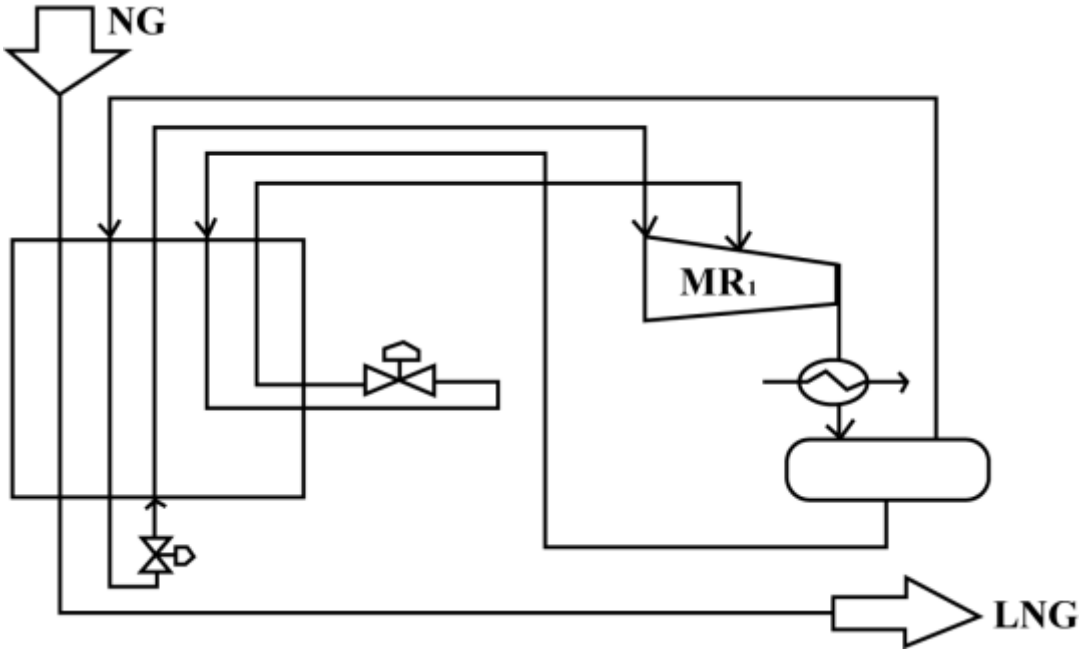

Fig.5 : Basic single flow LNG process for less than 0.2 mtpa LNG [Modified after 14,37].

4. LPG AND LNG PROSPECT IN BANGLADESH

LPG demand in Bangladesh has soared by 66% to around 500,000 mt/year in fiscal 2011-12, ended on June 30, 2012, compared with 300,000 mt/year in fiscal 2010-11. Before the suspension, LPG demand in the country was around 100,000 mt/year in fiscal 2010-11[17]. Thus, the total supply of LPG in the country by 2012 is about 121 thousand ton/year against a demand of 500 (Table.3).

Table.3: Status of LPG market in Bangladesh during 2012[17,26].

Sources of LPG	Amount(Ton per year)
Kailashtila fractionation plant, Golapgonj	7580
Eastern refinery Ltd, Chittagong	13200
Import by private sectors	100,000
Total supply	121,050

The Chittagong LPG plant has bottling capacity of 10,000 M.ton of LPG per shift per year though its average production is 13,000 M.ton per year over the last five years. The bottled LPG is being marketed through three marketing companies of BPC. The other plant of the company at Kailashtila, Sylhet has been bottling over 7,000 M.tons per year. This company on an average has been supplying over 20,000 M.tons of LPG to various parts of the country which is roughly 15%-20% of the current demand and private players import the remaining 80 percent [7, 36].The demand of LPG in Bangladesh increasing because it is cost effective, accessible, clean burning, excellent safety and easily transported facilities. Only about 10% fortunate persons of Bangladesh are blessed with pipeline gas supply and about 90% have to use alternate fuel [3, 7, 28, 36].

The average LPG consumption value for Bangladesh during that period was 0.54 thousand barrels per day with a minimum of 0.28 thousand barrels per day in 1992 and a maximum of 1.31 thousand barrels per day in 2003(Fig.6) [39]. The LPG consumption value for Bangladesh during 2001 to 2010 is given below figure.

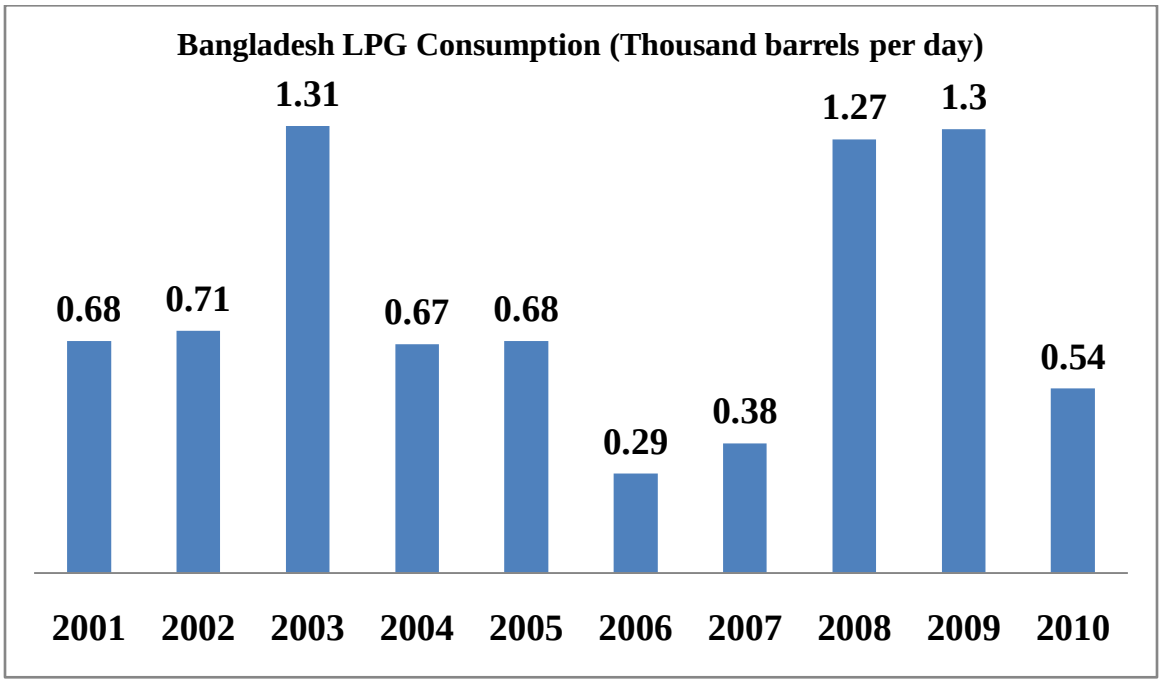

Fig.6: LPG consumption in Bangladesh [39].

Otherwise, there is no sufficient supply of gas in Bangladesh and the gas demand increasing day by day. If additional supply is available gas users even in Southern region can be benefited through setting up gas based industries. Now a days to meet immediate requirement of natural gas, LNG is the main source of supply. Bangladesh will definitely require importing LNG to support its natural gas sector for long term gas supply security [28].

Bangladesh is proceeding with a plan for setting up a 3.5 million tonnes a year LNG import facility at Matarbari in Maheshkhali Island of Cox's Bazar district or Anwara, Chittagong. In Bangladesh, as the port facilities is very limited and specially for LNG vessel because of the higher requirement of draught, it has been planned to use FSRU (Floating Storage and Re-gasification Unit) near Moheshkhali where required draught is available at about 5-6 km offshore of Moheshkhali coast. The mother vessel carrying LNG would be transferred to the FSRU which would be moored at about 5-6 km off-coast of Moheshkhali. An offshore pipeline would be installed from the FSRU and a delivery point will be stationed on-shore at Moheshkhali Island. From the delivery point, a gas transmission pipeline of about 85-90 km would be installed to bring the gas at the port city of Chittagong. In Chittagong, it would be hooked up with Karnaphully gas system and the gas would be supplied to the customers. It is estimate that 4 million ton of LNG would be required annually [3,4,19,33].

5. COMPARSION LPG AND LNG DEMANDS OF BANGLADESH WITH OTHERS COUNTRY

The demand of LPG is increasing day by day in the world. Total LPG demand in Bangladesh is 100000 mt/year [26]. Whereas, Indian demand increasing from 18.6 million tons in 2014 to 19.2 million tons in 2015 and China imported 7.1 million tons of LPG through 2014 (propane, butane and mixed) as opposed to 4.2 million tons in 2013. Otherwise, in 2014 the USA exported about 14 million tons of LPG [34].The

largest LPG exporters are found in the Middle East, West Africa (primarily Algeria) and the North Sea (Norway), whilst the largest importers include Northeast Asia (Japan, China and South Korea), the USA and the EU(Fig.7) [5,11,12,34].

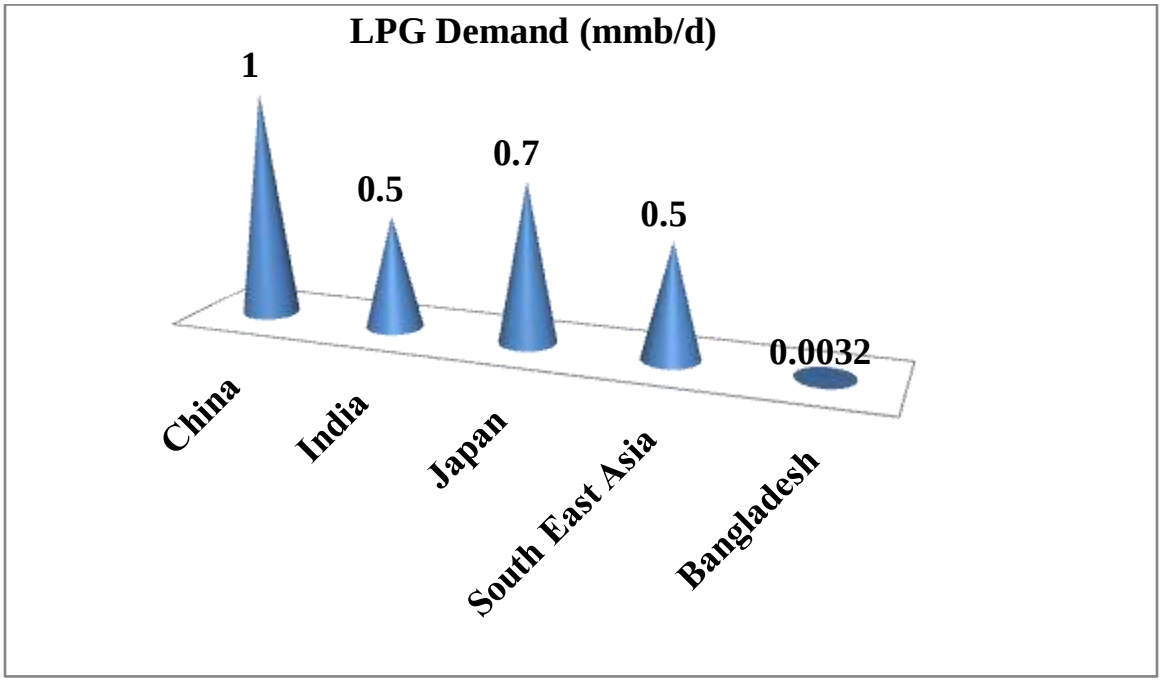

Fig.7: Comparison among LPG demands of Bangladesh with others largest importers country [44].

The world LNG demand is increasing year to year. It is estimate that 4 million ton of LNG would be required annually in Bangladesh. Demand for LNG will be heaviest in Asia Pacific, rising from the current 180 bcm to somewhere between 254 and 275 bcm by 2020. China and India will be the biggest players. China's demand for gas will climb up to 350 bcm by 2020. China's domestic gas production capacity of 210 bcm in 2020, with 70 bcm expected to come from unconventional gas sources. Consequently, China will need to import up to 140 bcm of gas in 2020, although it has already signed pipeline gas and LNG import contracts for a total 90 bcm of gas. In the Americas, LNG demand is not expected to increase significantly (Fig.8). In Europe, higher demand for LNG will be over this decade, from around 80 bcm to 113 bcm, an increase of 42 percent [31,32,39].

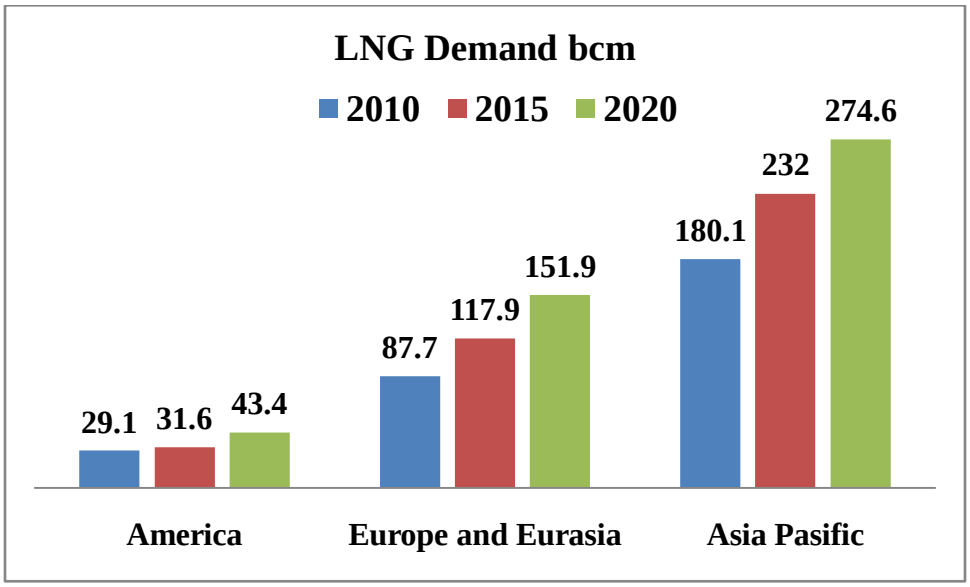

Fig.8: LNG demand (bcm) regionally [39].

6. LPG AND LNG OVER ALTERNATES

LP Gas is modern, safe and accessible everywhere without major infrastructure investment. LPG can be transported, stored and used virtually anywhere in the world. It is very clean burning, cost effective and has lower greenhouse gas emission than any other fossil fuel used in multi-purpose energy such as cooking, heating air condition, transportation. Compared to other fuels has an excellent safety record worldwide when handle properly and is non-toxic. It is produced either from wet natural gas in NGL fractional plant or in the crude oil refinery as a byproduct [1,17,18,42,43]. In Bangladesh the pipe line supply is not available in everywhere. Hence, the LPG is safe to use in this area [17].

LNG requires 600 times less space than natural gas. So, it is more economical to transport across large distances and can be stored in larger quantities. LNG is a price-competitive source of energy that could help meet future economic needs in the Bangladesh. It's a clear, colorless, odorless liquid. LNG is neither corrosive nor toxic and weighs less than half the weight of water. It is not explosive [14,17,18,42].

7. ECONOMIC VALUABLE OF LPG AND LNG FROM OTHER PETROLEUM REFINING PRODUCTS

Compressed Natural Gas or **CNG** is stored on the vehicle in high-pressure tanks - 20 to 25 MPa (200 to 250 bars, or 3,000 to 3,600 psi). Natural gas consists mostly of methane and is drawn from gas wells or in conjunction with crude oil production. As delivered through the pipeline system, it also contains hydrocarbons such as ethane and propane as well as other gases such as nitrogen, helium, carbon dioxide, sulphur compounds, and water vapors. A sulphur-based odorant is normally added to CNG to facilitate leak detection [6,24]. Natural gas is lighter than air and thus will normally dissipate in the case of a leak, giving it a significant safety advantage over gasoline or LPG. LNG is natural gas stored as a super-cooled (cryogenic) liquid. The temperature required to condense natural gas depends on its precise composition, but it is typically between -120 and -170°C (-184 and –274°F). The advantage of LNG is that it offers an

energy density comparable to petrol and diesel fuels, extending range and reducing refueling frequency. The disadvantage, however, is the high cost of cryogenic storage on vehicles and the major infrastructure requirement of LNG dispensing stations, production plants and transportation facilities. LNG has begun to find its place in heavy-duty applications in places like the US, Japan, the UK and some countries in Europe. For many developing nations, this is currently not a practical option [20,28,30]. Liquefied Petroleum Gas **(**also called Auto gas**)** consists mainly of propane, propylene, butane, and butylenes in various mixtures. It is produced as a by-product of natural gas processing and petroleum refining. The components of LPG are gases at normal temperatures and pressures. One challenge with LPG is that it can vary widely in composition, leading to variable engine performance and cold starting performance. At normal temperatures and pressures, LPG will evaporate. Because of this, LPG is stored in pressurized steel bottles. Unlike natural gas, LPG is heavier than air, and thus will flow along floors and tend to settle in low spots, such as basements. Such accumulations can cause explosion hazards, and are the reasons that LPG fuelled vehicles are prohibited from indoor parades in many jurisdictions. CNG is Compressed Natural Gas, which is mainly methane compressed at a pressure of 200 to 248 bars. LPG is Liquefied Petroleum Gas, a mixture of propane and butane liquefied at 15 °C and a pressure of 1.7 - 7.5 bar. Some variants of LPG are primarily propane so LPG is often colloquially called propane. CNG is cheaper and cleaner, but LPG has a higher calorific value. Distribution is easier for natural gas over long distances via pipelines. LPG is cheaper than diesel or gasoline. LPG vehicles have lower maintenance costs. It has lower emission than gasoline or diesel. It is non-toxic and non-corrosive. It requires lesser space than CNG for storage. Methane gas is processed into LNG by cooling it to −161°C, at which point it becomes a liquid. This reduces the volume of the natural gas by a factor of more than 600 times as it goes from its gaseous state to liquid. That's like going from a beach ball to a ping pong ball. This reduced volume facilitates economical transport by sea or road. Common LNG uses include industrial applications and long haul trucking [5,18,29,31,35,43].

8. CONCLUSIONS

To speed the process of encouraging the use of gas in the domestic use, especially the gas fired power generations; it has the option to invest in gas sector by offering low prices to gas consumers. The present world would encourage rapid consumption growth and in the replacement of oil products by gas. The expansion in gas power generation, the large number of new terminals and projects that have been proposed around the world and the expansion of the existing ones, no doubt, will increase competition not only among original suppliers, but also among new producers as well. Bangladesh should think about LPG & LNG option to meet the demand of natural gas. In the last decades, the world-wide LPG & LNG have growth significantly to meet the demand of natural gas allowing business opportunities. The cost and location advantages, however, are likely to persist in the world market of Bangladesh.

9. RECOMMENDATIONS

It is clear that energy is a crucial national issue, and natural gas is a valuable resource. The poverty-ridden country of Bangladesh, which is still struggling hard with its development, cannot afford to make mistakes regarding the utilization of natural gas. The following points are recommended:

I. Pipeline supply of natural gas for domestic and commercial user in small towns is already a bad economic choice in Bangladesh and it would be more appropriate to replace pipeline supply of natural gas by Liquefied Petroleum Gas in these places. It should be established an import based LPG storage and bottling plant under government-foreign-private partnership in different place of the Bangladesh.

II. In order to supplement indigenous natural gas, it should be import LNG to bridge or minimize the demand-supply gap. Towards this end, it should be installed floating LNG terminals on Build, Own, Operate and Transfer (BOOT) basis at different Islands in the Bay of Bengal.

III. Regional co-operation is a major component of an efficient allocation of resources, as many of the energy resources yield optimal benefits when exploited by two or more countries based on their respective comparative advantage in gas production, processing, marketing, and distribution or utilization. Thus, effective and appropriate regional cooperation could be one possible solution to long-term energy provisions for the region in general and Bangladesh in particular. Bangladesh is strategically located between two major economic regions—South Asia and Southeast Asia. LPG and LNG technological benefits should also be shared through regional cooperation.

IV. At a high level, government should conduct integrated resource planning for the energy sector, including environmental and social objectives.

REFERENCES

1. Ahmad, R.M.; Majed, A.; Osama, E.D.H.; Marcos, S.F.; and Usman, M. A. Fractionation of Natural Gas Liquids to produce LPG. TPG4140 Natural Gas, Norway, 2011.
2. Alawode, A.J.; Omisakin,O.A. Monetizing Natural Gas Reserves: Global Trend, Nigeria's Achievements, and Future Possibilities. The Pacific Journal of Science and Technology. 2011, Volume 12. Number 1.
3. Ali, M. M. (2016). LNG Prospect in Bangladesh. http://ep-bd.com/online/details.php?cid=32&id=17538. It is a snapshot of the page as it appeared on 26 Sep 2016 09:32:31 GMT.
4. Asian Development Bank, Strengthening of the Hydrocarbon Unit in the Energy and Mineral Resources Division (Phase II), Petroleum Refining & Marketing (Package # 06, Recommendation report on Policy and Regulation,C1334 – January 2012,RFP HCU/CS-06.
5. Alternative fuels and infrastructure in seven non-EU markets - Final report. Contract: MOVE/C1/SER/2014-268 21, January 2016.
6. Baker,R.W.,2002. Future Directions of Membrane Gas Separation Technology. Ind. Eng. Chem. Res. 2002, 41, 1393-1411.
7. Bangladesh Petroleum Corporation (BPC), LP Gas Limited, 2016 (Accessed on 01 October, 2016).
8. Cheang,C.Y. (2016). Petrobangla, Excelerate Sign Agreement to Build Bangladesh's First FSRU. Rigzone News. Published. Monday, April 04, 2016
9. Chowdhury, M. N. M.; Uddin, S.; Saleh,S. Present Scenario of Renewable and Non-Renewable Resources in Bangladesh: A Compact Analysis. International Journal of Sustainable and Green Energy. 2014, Vol. 3, No. 6, 2014, pp. 164-178.
10. Cuellar, K. T.; Hudson, N. M. and Wilkinson, J. D. Economical Options for Recovering NGL/LPG at LNG Receiving Terminals. Proceedings of the 86th GPA Annual Convention. 2007, Pp. 2-10.
11. Dahan, A. A. Natural Gas of Yemen the Challenge of Growth in the World's Gas Markets. World Journal of Social Sciences. 2011,Vol. 1. No. 2. May 2011 Pp. 146 – 157.

12. Danish Ship Finance A/S, 2012. Shipping Research, Demand – LNG (Accessed on 28 September, 2016).
13. Domestic gas prices up 50pc. Independent Publications Limited at Media Printers, Dhaka, Bangladesh. Last Modified: 29 August, 2015 12:44:44 AM.
14. Eldar,K.; Feby,F. and Juejing,S. Process Design and Economic Investigation of LPG Production from Natural Gas Liquids (NGL). TKP4170 Process design, Norway, 2010.
15. Elgas Ltd. (2016). http://www.elgas.com.au (Accessed on 25 September, 2016).
16. Gomes, I. Natural Gas in Pakistan and Bangladesh: current issues and trends. Oxford Institute for Energy Studies, NG77, June, 2013.
17. Imam,B. Energy Resources of Bangladesh. ISBN 984-809-020-1. The University Grants Commission of Bangladesh, Dhaka, January 2013.
18. International Association of Oil & Gas Producers. OGP, Regulators's use of standards, Report No. 426, March 2010.
19. Islam,S.; Muzemder, A.T.M.S.H. An Overview on LNG Business and Future Prospect in Bangladesh. Science Journal of Energy Engineering, 2015; 3(5): 40-45.
20. Japan will continue to dominate Asian LNG picture. Oil & Gas Journal. 07-07-2003.
21. 15.Jensen, J.K. The LNG revolution. The Energy Journal. 2003, vol. 24, no. 2, pp. 1–45.
22. Karim,M. (2016).Encouraging the use of LPG by households. Published: April 28, 2016 Thursday 12:17 PM BdST. Energynewsbd.com, Dhaka, Bangladesh.
23. LNG as ship fuel, The future – TODA ., DNV GL ,No 01 2014
24. Membrane Technology and Research (MTR), Inc., 2016. LPG Recovery From Associated gas: LPG-SEP™ (Accessed on 28 September, 2016).
25. Miah, M.I. and Howladar, M.F. Natural Gas Properties Analysis of Bangladesh: A Case Study of Titas Gas Field. SUST Journal of Science and Technology. 2012, Vol. 16, No.2, P:26-31.
26. Ministry of Power, Energy and Mineral Resources (MPEM), 2016 (Accessed on 01 October, 2016).
27. Ministry of Power, Energy and Mineral Resources (MPEM). 2008. National Energy Policy, Draft report, Dhaka.
28. Mujeri, M.K.; Chowdhury, T.T. and Shahana, S. Energy Sector in Bangladesh: An agenda for reforms. GSI REPORT, International Institute for Sustainable Development, 2014.
29. National Petroleum Council, 2003. Balancing natural gas policy: Fueling the demands of a growing economy, Task group report and LNG subgroup report, National Petroleum Council.
30. Oil and Gas Reality Check 2015, A look at the top issues facing the oil and gas sector.
31. Organization of Arab Petroleum Exporting Countries, Prospects for Growth of the Gas Industry, Trends and Challenges, Issue No.103, Volume 28 of the Oil and Arab Cooperation.
32. Parikh, J.; Purohit, P.; Maitra, P. Demand projections of petroleum products and natural gas in India. Energy. 2007,Volume 32, Issue 10, Pages 1825–1837.
33. Petrobangla, Bangladesh Oil, Gas and Mineral Corporation, Annual Report,2015.Dhaka, Bangladesh.
34. Poten & Partners. LPG in the world market, A Monthly Report on International Trends in LPG, February,2015.
35. Raheem, A.B.; Hassan, A.; Samsudin, S.A.; Noor, Z.Z.; Adebobajo, A. Comparative Economic Investigation Options for Liquefied Petroleum Gas Production from Natural Gas Liquids. American

Journal of Chemical Engineering. Special Issue: Developments in Petroleum Refining and Petrochemical Sector of the Oil and Gas Industry. 2015, Vol. 3, No. 2-1, 2015, pp. 55-69.

36. Saleque, K.A. LPG- Potential alternative. Energy and Power, 2003, v.1, Issue 4, p.10-15
37. Simon,H.D.,2007. LNG, LP and GTL plants Industrial gases and cryogenic applications. V12,Samson ag mess - UND regeltechnik, Weismüllerstraße 3,60314 Frankfurt am Main,Germany, 2007-10-29/V 1.7
38. Union Gas Limited, A Spectra Energy Company, Canada.,2016 (Accessed on 01October, 2016).
39. U.S. Energy Information Administration / Monthly Energy Review August 2016.
40. Wadus, Z.; Dey, H.S.; Kabir, M.A. and Khan, S.I. Modeling for forecasting natural gas demand in Bangladesh. Energy Policy, 2011, 39(11).7372-7380. ISSN 0301-4215.
41. Vink, K.J., and Nagelvoort, R.K., 1998. Comparison of Base load Liquefaction Processes, Paper presented at the 1998 Intl. Conference on Liquefied Natural Gas, Perth, Australia, 4–7 May.
42. Welcome to Country Report Presentation on Energy Scenario of Bangladesh. 8 May,2012. IEEJ: May 2012.
43. Wilkinson, J.D.; Hudson, H. M.; Cuellar, K.T. and Pitman, R.N. Next Generation Processes for NGL/LPG Recovery, Proceedings of the 77th GPA Annual Convention. 2002, pp 1-8.
44. World Energy Consultants, LLC – 2016 (Accessed on 28 September, 2016).
45. Wadud, Z.; Dey, H.S.; Kabir, M.A. and Khan, S.I. Modeling and forecasting natural gas demand in Bangladesh. Energy Policy. 2011, 39 (11). 7372 - 7380.

International Conference on Petroleum Engineering 2016 (ICPE-2016)
Bangladesh University of Engineering & Technology (BUET)
Dhaka-1000, Bangladesh

ICPE (2016-018)

Natural Gas Dehydration Process in Bangladesh

Md. Mehedi Hasan[1*], M Farhad Howladar[2], Abdullah Al Mahmud [1], Md. Bayezid Hussain[1]

[1]Department of Petroleum &Mineral Resources Engineering,Bangladesh University of Engineering & Technology (BUET),Dhaka, Bangladesh

[2]Department of Petroleum and Mining Engineering, Shahjalal University of Science and Technology, Sylhet, Bangladesh

ABSTRACT

Dehydration of natural gas is needed to remove the water that is associated with natural gases in vapor form. The natural gas industry has recognized that dehydration is necessary to ensure smooth operation of gas transmission lines. Dehydration prevents the formation of gas hydrates and reduces corrosion. Unless gases are dehydrated, liquid water may condense in pipelines and accumulate at low points along the line and reducing its flow capacity. Several methods have been developed to dehydrate gases on an industrial scale. The three major methods of dehydration are direct cooling, adsorption, and absorption. In Bangladesh 21 out of 26 gas field are producing nearly 2700 MMCFD gas with 13000 BBL condensate. Dehydration method, selected based on the gas property and location of gas field as well as customer demand. Most of the gas Field in Bangladesh are using Glycol (89 %) to dehydrate gas other used solid desiccant (Silica Gel, Molecular Sieve, 9 %) and (LTS, LTX, 2%). Glycols used for dehydrating natural gas in Bangladesh is , triethylene glycol (TEG),which has universal acceptance as most cost effective due to its superior dew point depression, operation cost and operation reliability. Solid desiccant (Silica, molecular sieve) type dehydration is a very simple process, ideal for remote locations with limited utilities, environment benefit, easy to install and operate and it also suitable in laboratory scale. Considering economical, gas composition, government rules presently the gas company are facing few problem in both processing, which are need to solve by taking proper action by government.

Key Words: Natural gas, Dehydration, Glycol, Silica Gel, Bangladesh.

* Corresponding Author address
Email: mehedipge06@yahoo.com

INTRODUCTION

Today, natural gas is one of the most important fuels in our life and one of the principle sources of energy for many of our day-to-day needs and activities. It is important factor for the development of countries that have strong economies because natural is the source of energy for household, industrial and commercial use, as well as to generate electricity. It is one of the cleanest, safest, and most useful of all energy sources. It consisting primarily of methane but including significant quantities of ethane, propane, butane, and pentane and other impurities such as carbon, sulfur, nitrogen, water etc at reservoir because of high pressure and temperature. Natural gas is considered 'dry' when it is almost pure methane, having had most of the other commonly associated hydrocarbons removed. When other hydrocarbons are present, the natural gas is 'wet'[5]. In order to meet the requirements for a clean, dry, wholly gaseous fuel suitable for transmission through pipelines and distribution for burning by end users, the gas must go through several stages of processing, including the removal of entrained liquids from the gas, followed by drying to reduce water content [6].

In order to remove water content, dehydration process is used to treat the natural gas. Dehydration (hypohydration) is the removal of water from an object. In Physiologic terms, it entails a relative deficiency of water molecules in relation to other dissolved solutes. Gas dehydration is one of the most prominent unit operations in the natural gas industry. In this operation water, content is removed from natural gas streams to meet sales specifications or other downstream gas processes such as gas liquid recovery

OBJECTIVE

The objective of the paper is to find out different natural gas processing system in Bangladesh and its limitation and problem in each gas processing system.

TYPES OF DEHYDRATION OF NATURAL GAS

Dehydration of natural gas is the process removal of the water that is associated with natural gases. The natural gas industry has recognized that dehydration is necessary to ensure smooth operation of gas transmission lines. Several methods have been developed to dehydrate gases on an industrial scale. The four major methods of dehydration are adsorption, absorption gas permeation and refrigeration [1, 2]. Absorption dehydration involves the use of a liquid desiccant to remove water content from the gas. Although many liquids possess the ability to absorb water content from gas, the liquid that is most desirable to use for commercial.

Adsorption (or solid bed) dehydration is the process where a solid desiccant is used for the removal of water content from a gas stream. The solid desiccants commonly used for gas dehydration are those that can be regenerated and, consequently, used over several adsorption-desorption cycles. The mechanisms of adsorption on a surface are of two types; physical and chemical. The latter process, involving a chemical

reaction, is termed "chemisorption". Chemical adsorbents find very limited application in gas processing. Adsorbents that allow physical adsorption hold the adsorbate on their surface by surface forces.
The most widely used adsorbents today are activated alumina, silica gel, molecular sieves (zeolites). A hydrated form of aluminum oxide (Al2 O3), alumina is the least expensive adsorbent. It is activated by driving off some of the water associated with it in its hydrated form ((Al2 O3.3H2 O) by heating. It produces an excellent dew point depression values as low as -100 ^{0}F, but requires much more heat for regeneration

There are numbers of liquids that can be used to absorb water from natural gases such as calcium chloride, lithium chloride and glycols. Glycol dehydration is a liquid desiccant system for the removal of water from natural gas. It is the most common and economic means of water removal from these streams [11]. Glycol, the principal agent in this process, has a chemical affinity for water. The liquid glycol will absorbs the water content in the natural gas. This means that, when in contact with a stream of natural gas that contains water, glycol will serve to 'steal' the water out of the gas stream. This operation is called absorption. [4]

There are a few types of glycol usually used in industry with their advantages and disadvantages like ethylene glycol (EG), diethylene glycol (DEG), triethylene glycol (TEG), and tetraethylene glycol (TREG). One of the best glycol frequently used in industry is TEG. Essentially, glycol dehydration involves using a glycol solution, usually either DEG or TEG, which is brought into contact with the wet gas stream in what is called the 'contactor' or dehydration unit. The process function of glycol is absorbing the water from the wet gas. Once absorbed, the glycol particles become heavier and sink to the bottom of the contactor where they are removed.Usually, TEG is used because it is the most commonly used glycol in industry. TEG is used as absorber of water content in natural gas [12].TEG, or triglycol is a colourless, odourless viscous liquid with molecular formula C6H14O4 and molecular structure [3,4] .Although many liquids possess the ability to absorb water from gas, the liquid that is most desirable to use for commercial dehydration purposes should possess the following properties [11]:

- Strong affinity for water
- High boiling points
- Low cost.
- Noncorrosive
- Low affinity for hydrocarbons and acid gases
- Thermal stability.
- Easy regeneration
- Low viscosity
- Low vapor pressure at the contact temperature
- Low solubility in hydrocarbon.
- Low tendency to foam and emulsify.

Md. Mehedi Hasan[1*], M Farhad Howladar[2], Abdullah Al Mahmud [1], Md. Bayezid Hussain[1]

OVERVIEW OF NATURAL GAS INDUSTRIES IN BANGLADESH

There are 26 discovered gas field in Bangladesh among 21 are at operated condition producing nearly 2700 MMSCFD gas and 13000 BBL condensate which is less than our total demand per day [13]. The natural gas in Bangladesh consider as pure gas because it contain nearly 95 % methane and small amount of ethane and propane without containing any sulfur. The chemical composition of natural gas in different gas field almost similar in every gas field. The chemical composition of natural gas in different gas field are given at table 1

Table 1: Chemical Composition of Natural Gas in Bangladesh at Different gas field. [7]

Name of Gas Field	Chemical Composition of Gas (Volume Percent)								
	Methane	Ethane	Propane	ISO Butane	N-Butane	High Composition	N_2	CO_2	SG
Haripur	96.63	2.0	.05	0.14	0.01	0.17	0.66	0.34	0.55
Kailashtilla	95.57	2.70	0.94	0.21	0.20	0.14	0.24	-	0.59
Rashidpur	98.0	1.21	0.24	-	-	0.17	0.02	0.05	0.57
Beanibazar	93.68	3.43	1.10	0.29	1.23	0.17	0.99	0.12	1.60
Chattak	97.90	1.80	0.20	-	-	-	-	-	0.55
Titas	97.33	1.72	0.35	0.08	0.05	0.06	0.30	0.11	0.57
Habiganj	97.60	1.31	0.27	0.08	0.04	0.06	0.38	0.07	0.57
Bakhrabad	94.20	3.65	0.72	0.20	0.10	0.24	0.42	0.47	0.60
Narsingdi	94.79	2.49	0.60	0.20	0.15	0.13	0.34	0.60	0.61
Meghna	95.15	2.83	0.60	0.16	0.09	0.07	0.37	0.53	0.59
Kamta	95.36	3.57	0.47	0.09	-	-	-	0.51	0.57
Sangu	94.51	3.17	0.61	0.19	0.07	0.41	0.44	0.60	0.59

Saldanadi	96.32	2.16	0.45	0.12	0.07	0.05	0.27	0.56	0.57
Fenchuganj	95.66	2.50	0.63	0.11	0.04	-	-	0.06	0.57
Shahbazpur	93.68	3.94	0.71	0.20	0.07	0.04	0.46	0.90	0.58
Semutang	96.94	1.70	0.14	-	0.01	-	0.86	0.35	-
Begumganj	95.46	3.19	0.64	0.17	0.04	-	-	0.30	0.58
Bibiyana	95.46	2.40	1.08	0.22	0.19	0.30	0.20	0.15	-

NATURAL GAS PROCESSING SYSTEM IN BANGLADESH

Both adsorption, absorption method are using in Bangladesh for Dehydrate natural gas. For adsorption, silica gel and molecular sieve are used. Sylhet gas Field ltd as well as Bakharabad and Fenchugonj, Srikail gas field are the main user of the solid desiccant (Table 2), where other gas fields are using absorbent like TEG, MEG [8,9,10]. Nearly 89 % gas of total production are dehydrate using glycol where silica gel user are only 7 % and 2% using LTX or LTS. (Figure: 1)

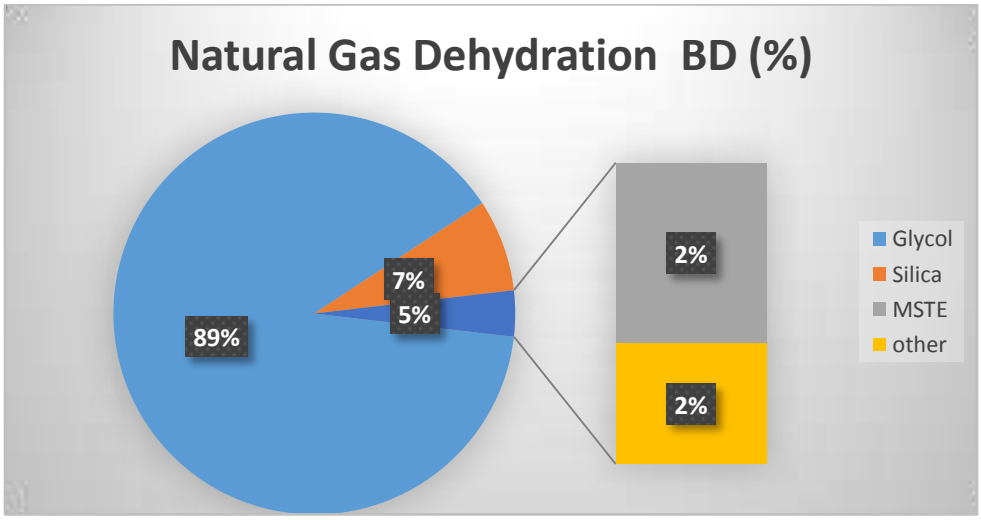

Figure 1: Natural Gas Dehydration process in Bangladesh. [7, 8, 9]

Table 2: Natural Gas Processing System in Bangladeshi Gas Field [7, 8, 9]

Company	Gas Field	Capacity	Process System
	Haripur Field	1X30 MMSCFD.	Silica Gel
	Kailashtilla Field	1X30 MMSCFD.	Silica Gel
		2X45 MMSCFD,	Silica Gel

Sylhet Gas Field Ltd	Rashidpur Field	1X70 MMSCFD. 1X60 MMSCFD	Silica Gel TEG
	Beanibazar Field	1X60 MMSCFD	Silica Gel
	Kailashtilla Field II	1 x 90 MMSCFD	Molecular Sieve
	Chattak Gas Field	1X10 MMSCFD	TEG
BGFCL	Titas Gas Field	Total 14 Capacity 810 MMSCFD	TEG (8) Low Temperature Separation (LTS) (4) LTS + Glycol (2)
	Habiganj Gas Field	420	TEG (6)
	Bakhrabad Gas Field	60 x 4 MMSCFD	Silica Gel
	Narsingdi Gas Field	1 x 60 MMSCFD	TEG
	Meghna Gas Field	1x 20 MMSCFD	Low Temperature Extraction (LTX)
	Kamta Gas Field	Production Suspended	
	Sangu Gas Field	Production suspended	
BAPEX	Saldanadi Gas Field	1X 20 MMSCFD	TEG
	Fenchuganj Gas Field	1X 60 MMSCFD	Silica Gel
	Shahbazpur Gas Field	2X35 MMSCFD	TEG
	Semutang Gas Field	1X30 MMSCFD	TEG
	Srikail Gas Field	1X60 MMSCFD	Silica Gel
	Begumganj Gas Field	1X20 MMSCFD	TEG
	Shahjadpur–Sundalpur Gas Field	1X20 MMSCFD	Early Production Facility
	Rupganj Gas Field	1X30 MMSCFD	TEG
	Mubarokpur Gas Field	Under Drilling Operation	
IOC			
Chevron Bangladesh	Bibiyana Gas Field	Capacity 1300 MMSCFD	TEG
	Jalalabad Gas Field	Capacity 350 MMSCFD	EG
	Moulavibazar Gas Field	1X60 MMSCFD	TEG
KrisEnergy	Bangora	1X60 MMSCFD	Silica gel

COMPARISON OF DEHYDRATION PROCESSES

There are a number of factors that must be considered when evaluating dehydration processes. However, in this project the comparison will be made on bases of advantages and disadvantages.

Advantages of using adsorption over absorption [14, 2, 15, 16, 17, 18]

1. Simplicity of design and operation of units
2. Insensitivity to moderate changes in gas temperature, pressure, flow rate, etc

3. Very low dew point temperatures can be achieved(<-50°C) that's a water content of less than 0.038 g/m3
4. They are less affected by small changes in gas pressure, temperature and flow rate
5. Generally free from corrosion and foaming problems
6. Ability to dehydrate very small quantities of gas at a low cost
7. Need to replace after two or three years

Disadvantages of using adsorption over absorption [16, 17, 18]

1. Higher costs in terms of adsorbent replacement compared to glycol replacement
2. It requires more space and weighs more compared to the absorption process.
3. Quality product may not be available due to government rule and regulation in Bangladesh

Advantages of using absorption over adsorption [14, 2, 15, 16, 17, 18]

1. Glycols are cheaper than adsorbents (silica gels, molecular sieves)
2. It is also cheaper to replace glycol than replace an adsorber bed
3. Lower installation costs; it is known that adsorption plants costs 50%more at 10MMscfd(million standard cubic feet per day) and 33% more at 50MMscfd
4. They have a lower pressure drop; -0.344 to 0.67 bars and 0.67 to 3.5 bar for adsorption.
5. Minimal glycol losses
6. Glycol systems are more continues and very viable for high flows as compared to adsorption.

Disadvantages of absorption over adsorption [14, 15, 2, 16, 17]

1. Achieving a water dew point less than – 32°C (water content of 0.244g/m3) is difficult and requires special design.
2. It becomes corrosive when it is decomposed as a result of excessive high temperatures
3. Need regular recharge.
4. Quality product may not be available due to government rule and regulation in Bangladesh

CONCLUSION

Dehydration of natural gas is important because without dehydring the natural gas may causes a corrosion and erosion problem during transmission and distribution of natural gas .Though the installation of adsorbent type dehyding process is costly with respect to absorbent type process its has benefits during dehydarate natural gas when dew point , foming and corrosion are main considerable . Considering the gas composition, most of the gas field in Bangladesh are using Glycol based process plant, which are cheaper than silica based process plant but need to continuous recharge.But due to government purchase rules and regulation the gas producing company uder Petrobangla facing some problem during gas dehydration. The government should take necessary steps to resolve the problem during gas dehydration by adsorption and absorption process.

REFERENCES

1. Christensen D. L. "Gas Dehydration, Thermodynamic simulation of the water/glycol mixture" MSc Thesis, Aalborg university Esbjerg,2009
2. Karnouskos P. "Investigation of the expansion of the natural gas network and uses in Greece, as well as the impendent need for carbon capture and sequestration "MSc Thesis, University of Strathclyde,2005
3. MOHAMAD A. S. "Natural Gas Dehydration Using Triethylene Glycol (TEG)" BSc Thesis, University Malaysia Pahang, 2009
4. Zangana F.S. A "A study of the dehydration process of natural gas in Iraqi North Gas Company and the treatment methods of molecular sieve problems" Higher Diploma , Thesis, University of Technology,2012
5. https://stateimpact.npr.org/pennsylvania/tag/natural-gas-prices/ (Accessed 7 September 2016)
6. https://www.google.com.hk/?gws_rd=ssl#q=dry+gas+definition (Accessed 7 August 2016)
7. https://www.titasgas.org.bd/temp/source/Gas_Composition.pdf (Accessed May 29, 2016)
8. https://www.google.com.hk/?gws_rd=ssl#q=bgfcl (Accessed 10 may 2016)
9. http://www.bapex.com.bd/?page_id=24 (Accessed 10 may 2016)
10. https://www.google.com.hk/?gws_rd=ssl#q=sylhet+gas+field (Accessed May 2, 2016)
11. Gas Dehydration (ENGINEERING DESIGN GUIDELINE), KLM Technology Group http://www.klmtechgroup.com/PDF/EDG/ENGINEERING_DESIGN_GUIDELINES_GAS_DEHYDRATION_Rev01web.pdf
12. http://en.citizendium.org/wiki/Glycol_dehydration (Accessed September 7, 2016)
13. http://www.petrobangla.org.bd/?C=M;O=A (Accessed may 26, 2016)
14. http://petrowiki.org/Dehydration_with_glycol (Accesed September 7, 2016)
15. http://www.premen.ru/en/content/gas/dry/ (Accessed June 30 ,2016)
16. http://inzynieriaaparaturachemiczna.pl/pdf/2010/20102/InzApChem_2010_2_87-88.pdf (Accessed September 7, 2016)
17. https://www.scribd.com/doc/6784934/Gas-Dehydration-Basics (Accessed 7 September 2016)
18. http://www.docstoc.com/docs/document-preview.aspx?doc_id=20187082 (Accessed September 6 ,2016)

International Conference on Petroleum Engineering 2016 (ICPE-2016)
Bangladesh University of Engineering & Technology (BUET)
Dhaka-1000, Bangladesh

ICPE (2016-040)

A Research of Material Balance Equation Applied to Natural Gas Liquefaction Process Considering Three Stage Cooling Section

Mohammad Shahedul Hossain [1,*]***, Jumman Al Jawad*** [1]
[1] Department of Petroleum & Mining Engineering,
Shahjalal University of Science & Technology, Sylhet-3114, BANGLADESH

ABSTRACT

This research paper deals with modern natural gas liquefaction technology and presents a material balance calculation model for an entire LNG liquefaction section which makes it possible to balance all streams in and out under particular conditions. This research focuses on the general conservation equation for any process system and this general formula was applied to five different sections of natural gas liquefaction process containing de-ethanizer section, de-propanizer section, de-butanizer section, N_2 rejection section and mixing section. All these sections were calculated separately during material balance calculation approach, as well as mole fraction, mass fraction, mass flow rate and molar flow rate of each, are calculated very precisely determining few specific assumptions which can be modified in later case upon availability of data and desired output. Result replicate that after material balance calculation, at each step and for every stream, when the error percentage was calculated almost all the streams gave no error or very minor percentages, and as expected, for each stream input was equal to output since there are no reactions. This research work will provide not only excellent support while simulating and analyzing LNG project operation but also will indicate distinct way of future adjustment with the modification of our prepared material balance sample based on further updated data and desired output.

Keywords: LNG liquefaction, Material Balance, Liquefaction Frationation Column, LNG stream flow, Three stage cooling

INTRODUCTION

The material balance is the central tool of chemical engineering which is the origin for the analysis and design of chemical processes. In chemical processing we deal with the transformation of raw materials into products and in many cases unwanted by-products that must be disposed of. The material balance is the tool for keeping track of what is entering and leaving the process as well as what goes on internally. Without accurate material balances, it is impossible to design or operate a chemical plant safely and economically [1].

* Corresponding Author address
E-mail: shahedulhossain@gmail.com

The general conservation equation for any process system can be written in the following balance equation:

$$Accumulation = Material\ in - Material\ Out + Generation + Consumption \quad (1)$$

For LNG which is a steady state process considering sweet natural gas as a feed, the accumulation term is zero.
Moreover, as there are no reactions, mass is neither generated nor consumed. The general conservation equation balance reduces to:

$$Material\ in = Material\ Out \quad (2)$$

Material Balance Method

Material Balance calculations are conducted to obtain all the missing material data for the LNG process. Unknowns such as (mass fractions, mass flow rates, mole fractions and mole flow rates) are found and calculated as they are required in the first step towards designing a world class LNG plant [2].
First step of the material balance procedure is to assume and determine some initial values of some of the unknowns to guide us and to start the calculations with. The LNG production rate was determined and the compositions of the feed, NGL and LNG streams were given initial values provided by supplying company.
Next, overall material balance equations are written in terms of mass fractions and mass flow rates and solved simultaneously using the known and assumed parameters to calculate for the remaining unknowns.

The step to follow is to do section by section material balance calculations to achieve two things, calculate and find the remaining unknown compositions and flow rates and to check and verify the overall material balance calculations at the same time. At each step and for every stream, the error percentage needs to be calculated. Almost all the streams gave no error or very minor percentages, and as expected, for each stream input was equal to output since there are no reactions.

Process Flow Diagram

While doing material balance calculations, two major decisions were taken to change the process and the process flow diagram slightly, as we believed they would help us in achieving the desired results and to make a better process. The first decision was to recycle back the upper streams of the De-propanizer (De-C_3), De-butanizer (De-C_4) and De-Pentanizer (De-C_5) and to mix it with the upper stream of the De-ethanizer (De-C_2) before it enters the cooling cycles. Making this decision brought a huge benefit for both the material balance calculations and the process itself. By recycling the upper stream of these three distillation columns, the number of unknowns in the overall material balance was reduced significantly, which made the calculations much easier and straighter forward. While on process wise, having three different columns that separate C_2, C_3 and C_4 individually, gave an extra way to control the compositions in the product LNG stream and a flexibility of tuning these compositions based on the desired criteria [3].

Following figure shows the simplified Process Flow Diagram that is used in the material balance calculation.

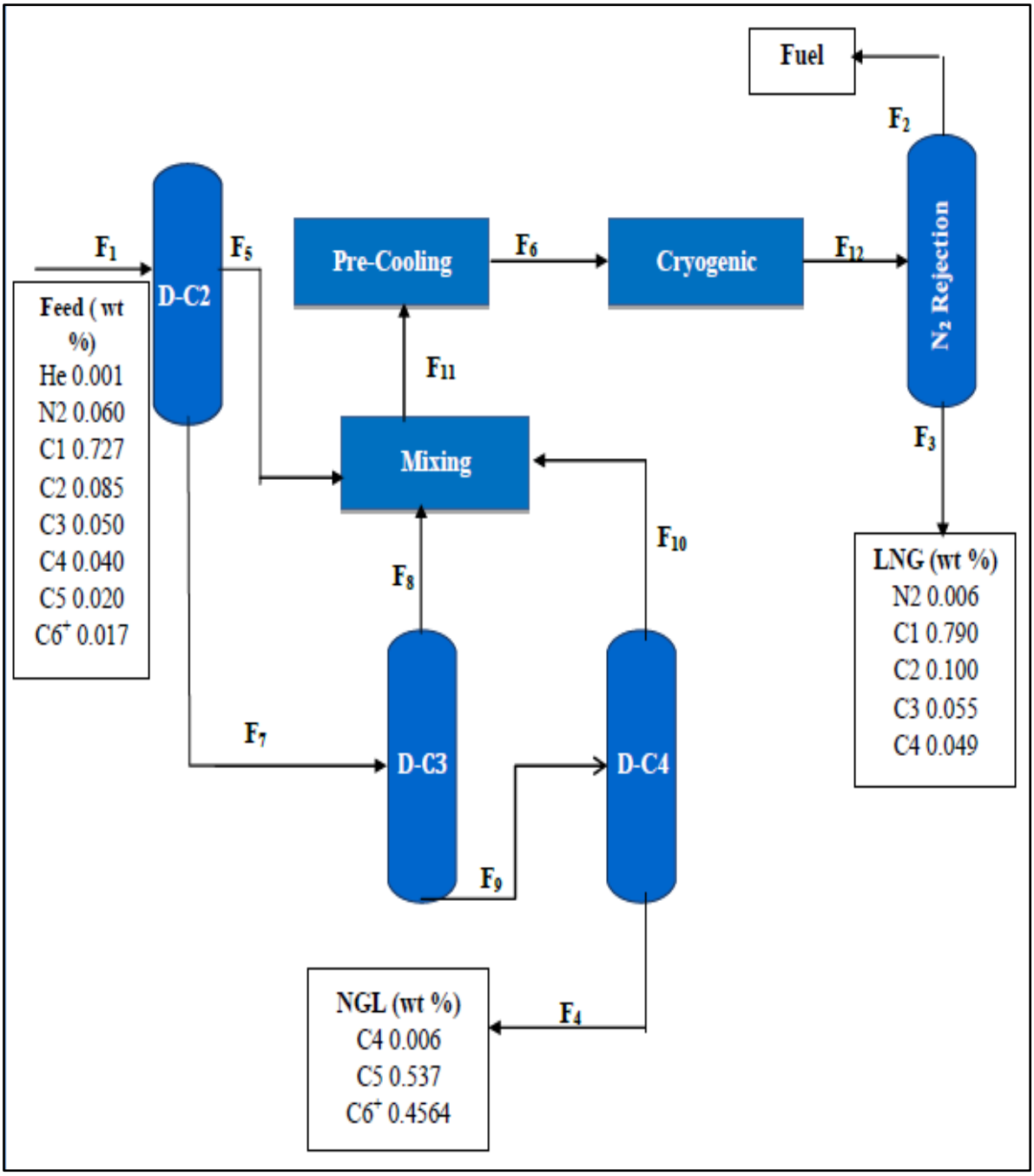

Figure 1: Simplified Process Flow Diagram

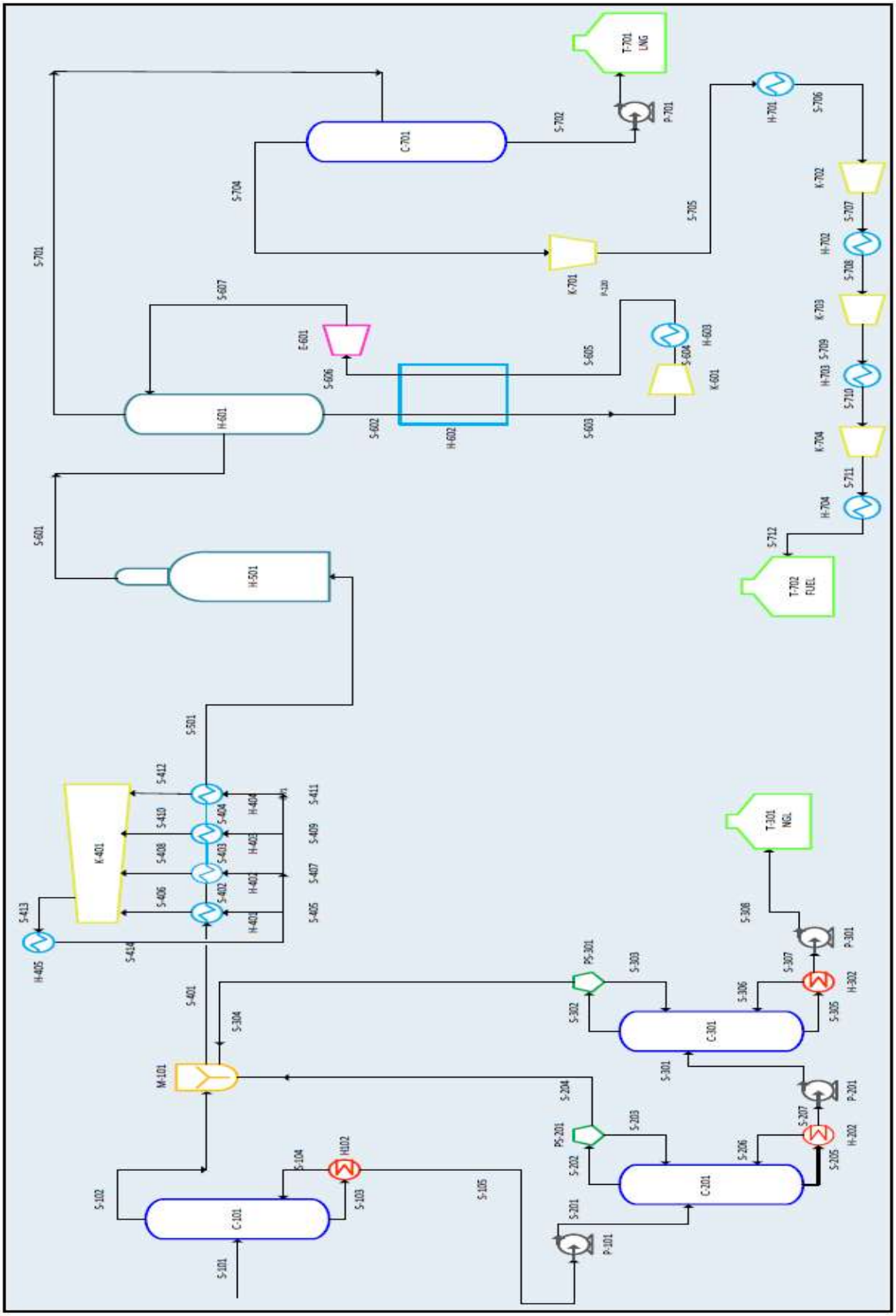

Figure 2**:** Final Process flow diagram for material balance [3]

ASSUMPTIONS

1. We will combine: i-C_4H_{10} & n-C_4H_{10}, i-C_5H_{12} & n-C_5H_{12};

And production Rate of 7.9 MTY (F_3) is considered for further modification.

2. N_2 Reject Top includes: He, N_2, CH_4, C_2H_6, & C_3H_8

3. For C_6+: Use C_6 (hexane) Molecular Weight for calculations

4. The tops of the distillation columns are recycled to the main stream entering the cooling section, so that the required composition of the product LNG is produced.

5. Inlet to the cooling sections (pre-cooling and sub-cooling) is the same as the outlet from it (i.e. Flow rates and composition of streams: S-401, S-501 and S-601 are equal).

6. For De-ethanizer:

a) Assume 99.9% of C_1 in the feed, 98% of C_2 in the feed and 100% of He & N_2 in the feed goes the top.

b) Assume 0.01% of C_1 in the feed, 2% of C_2 in the feed and 100% of C_3, C_4, C_5 & C_6+ in the feed goes to the bottom.

7. For De-propanizer:

a) Assume 99.9% of C_3 in the feed and 100% of C_1 & C_2 in the feed goes to the top.

b) Assume 0.01% of C_3 in the feed and 100% of C_4 & C_5 in the feed goes to the bottom.

8. For De-butanizer:

a) Assume 99.9% of C_3 in the feed and 100% of C_1 & C_2 in the feed goes to the top.

b) Assume 0.01% of C_3 in the feed and 100% of C_4 & C_5 in the feed goes to the bottom.

Material Balance Calculations

5.1 Specific Materials

Table 1: Considered streams composition for overall material balance

Component	Sweet Dry Gas (Feed) Mass Fraction	LNG (Product) Mass Fraction	NGL Mass Fraction
He	0.0001	0.00	0.00
N_2	0.060	0.006	0.00
C_1	0.727	0.790	0.00
C_2	0.086	0.1	0.00
C_3	0.050	0.055	0.00
C_4	0.040	0.049	0.006
C_5	0.020	0.00	0.537
C_6+	0.017	0.00	0.4564

5.2 Production Rate Conversion

Desired production Rate, F_3 = 7.9 MTY

Considering that there are normally 14 days of shutdown in a year, year = 351 days.

F_3 = 7.9 MTY

$$= 7.9 \times 10^6 \ \frac{ton}{year} \times \frac{907.2\ kg}{ton} \times \frac{1\ year}{351\ days} \times \frac{1\ day}{24\ hr} = 850769.23077 \ \frac{kg}{hr}$$

5.3 Overall Material Balance

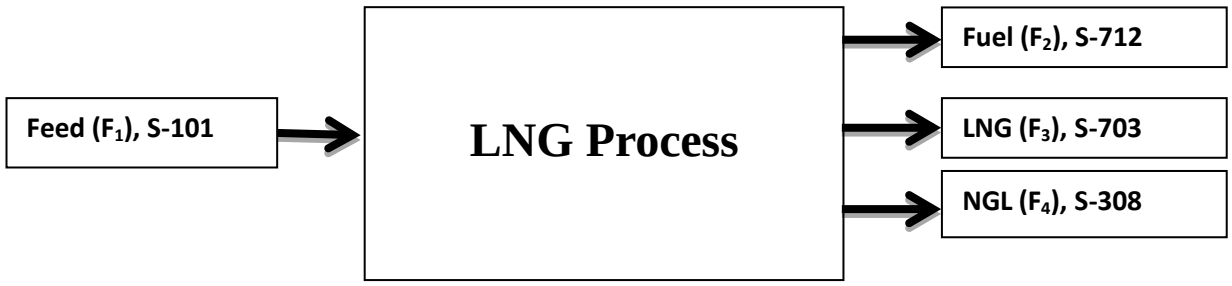

Figure 3: Overall material balance block diagram

The overall material balance is done using mass flow rates and composition.

Components of material balance from the overall block diagram:

C_1: $F_1C_{11} = F_2C_{12} + F_3C_{13}$
$0.727\ F_1 = F_2C_{12} + 0.79\ F_3$ (3)

C_2: $F_1C_{21} = F_2C_{22} + F_3C_{23}$
$0.086\ F_1 = F_2C_{22} + 0.79\ F_3$ (4)

C_3: $F_1C_{31} = F_2C_{32} + F_3C_{33}$
$0.05\ F_1 = F_2C_{32} + 0.055\ F_3$ (5)

C_4: $F_1C_{41} = F_3C_{43} + F_4C_{44}$
$0.04\ F_1 = 0.049\ F_3 + 0.006\ F_4$ (6)

C_5: $F_1C_{51} = F_4C_{54}$
$0.02\ F_1 = 0.537\ F_4$ (7)

C_6+: $F_1C_{61} = F_4C_{64}$
$0.017\ F_1 = 0.4564\ F_4$ (8)

N_2: $F_1N_1 = F_2N_2 + F_3N_3$
$0.06\ F_1 = F_2N_2 + 0.0006\ F_3$ (9)

He: $F_1H_1 = F_2H_2$

$0.0001\ F_1 = F_2H_2$ (10)

Overall: $F_1 + F_2 + F_3 + F_4$

$F_1 = F_2 + 850769.23077 + F_4$ (11)

From equation (7): $F_1 = 26.85\ F_4$

Substitute in equation (8):
$0.04\ (26.85\ F_4) = 0.049\ (850769.23077) + 0.006\ F_4$

From equations (6) and (7)
$F_1 = 1048047.321$ kg/hr , $F_4 = 39033.4198$ kg/hr

From equation (11):
$F_2 = 1048047.321 – 850769.23077 – 39033.4198 = 158244.6705$ kg/hr

From equation (5) :
$0.05\ (1048047.321) = C_{32}\ (158244.6705) + 0.055\ (850769.23077)$
$C_{32} = 0.0350$

From equation (4):

$0.086(1048047.321) = C_{22}\ (158244.6705) + 0.1(850769.23077)$
$C_{22} = 0.03194$

From equation (3):

$0.727(1048047.321) = C_{12}\ (158244.6705) + 0.79(850769.23077)$
$C_{12} = 0.56762$

From equation (10):
$0.0001\ (1048047.321) = H_2\ (158244.6705)$; $H_2 = 0.000662$

Composition of N_2 in the stream (N_2):
$N_2 = 1 – 0.0350 - 0.03194 – 0.5672 - 0.000662 = 0.36477$

Table 2: Calculated Mass Fractions and mole fractions for the overall material balance

Components	Mass Fractions				Mole Fractions			
	S-101	S-712	S-703	S-308	S-101	S-712	S-703	S-308
He	0.0001	0.0007	0.0000	0.00000	0.0005	0.0033	0.0000	0.0000
N_2	0.0600	0.3651	0.0060	0.00000	0.0406	0.2583	0.0039	0.0000
C_1	0.7270	0.5676	0.7900	0.00000	0.8609	0.7014	0.8974	0.0000
C_2	0.0860	0.0319	0.1000	0.00000	0.0543	0.0210	0.0606	0.0000
C_3	0.0500	0.0354	0.0550	0.00000	0.0215	0.0159	0.0223	0.0000
C_4	0.0400	0.0000	0.0490	0.00600	0.0130	0.0000	0.0153	0.0080
C_5	0.0200	0.0000	0.0000	0.53700	0.0052	0.0000	0.0000	0.5795
C_6+	0.0170	0.0000	0.0000	0.45640	0.0038	0.0000	0.0000	0.4124
Total	1.0001	1.0008	1.0000	0.99940	1.0000	1.0000	1.0000	1.0000

Table 3: Calculated Mass Flow Rate and Molar Flow Rate for the overall material balance

Components	Mass Flow Rate (Kg/hr)				Molar Flow Rate (kmol/hr)			
	S-101	S-712	S-703	S-308	S-101	S-712	S-703	S-308
He	104.8047	104.804	0.00000	0.00000	26.20118	26.20118	0.00000	0.00000
N_2	62882.83	57778.22	5104.6153	0.00000	2244.2126	2062.035	182.17757	0.00000
C_1	761930.4	89822.70	672107.69	0.00000	47501.895	5599.919	41901.975	0.00000
C_2	90132.06	5055.146	85076.923	0.00000	2997.4083	168.1126	2829.2957	0.00000
C_3	52402.36	5610.063	46792.307	0.00000	1188.5317	127.2411	1061.2907	0.00000
C_4	41921.89	0.00000	41687.692	234.2005	721.29891	0.00000	717.26931	4.02960
C_5	20960.94	0.00000	0.00000	20960.94	290.51901	0.00000	0.00000	290.51901
C_6+	17816.80	0.00000	0.00000	17814.85	206.76343	0.00000	0.00000	206.74078
Total	1048047.3	158244.6	850769.23	39033.41	55176.830	7983.509	46692.009	501.28939

Table 4: Percent Error for the overall material balance

Balance	Input (Kg/hr)	Output (Kg/hr)	Error (%)
Overall	1048047.32068	1048047.32068	0.000
He	104.80473	104.80473	0.000
N2	62882.83924	62882.83930	0.000
C1	761930.40214	761930.40214	0.000
C2	90132.06958	90132.06958	0.000
C3	52402.36603	52402.37164	0.000
C4	41921.89283	41921.89283	0.000
C5	20960.94641	20960.94641	0.000
C6+	17816.80445	17814.85278	0.011

5.4 De-ethanizer Column Unit Balance

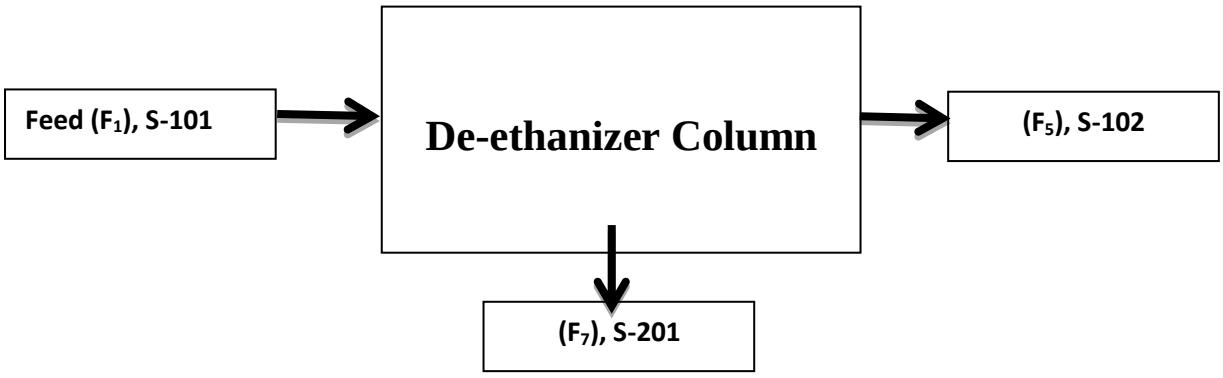

Figure 4: De-ethanizer column unit balance block diagram

Components Material Balance in distillate:

He: $F_1H_1 = F_5H_1 = 104.80473$ kg/hr

N_2: $F_1N_1 = F_5N_5 = 62882.83926$ kg/hr

C_1: $0.999F_1C_{11} = F_5C_{15} = 761168.47196$ kg/hr

C_2: $0.98F_1C_{21} = F_5C_{25} = 88329.42821$ kg/hr

Total mass flow rate of the distillate:

$F_5 = F_5H_1 + F_5N_5 + F_5C_{15} + F_5C_{25}$
$F_5 = 104.80473 + 62882.83926 + 761168.47196 + 88329.42821$ kg/hr
$F_5 = 912485.54417$ kg/hr
Component Mass fraction in distillate:

He mass fraction: $\frac{104.80473}{912485.54417} = 0.00011$

N_2 mass fraction: $\frac{62882.83926}{912485.54417} = 0.06891$

C_1 mass fraction: $\frac{761168.47196}{912485.54417} = 0.83417$

C_2 mass fraction: $\frac{88329.42821}{912485.54417} = 0.09680$

Components of material balance from the overall block diagram:

C_1: $F_1C_{11} = F_5C_{15} + F_7C_{17}$
$F_7C_{17} = 761930.40237 - 761168.47196 = 761.93040$ kg/hr

C_2: $F_1C_{21} = F_5C_{25} + F_7C_{27}$
$F_7C_{27} = 90132.06961 - 88329.42821 = 1802.64139$ kg/hr

C_3: $F_1C_{31} = F_5C_{35} + F_7C_{37}$
$F_7C_{37} = 52402.36605 - 0.00000 = 52402.36605$ kg/hr

C_4: $F_1C_{41} = F_5C_{45} + F_7C_{47}$
$F_7C_{47} = 41921.89284 - 0.00000 = 41921.89284$ kg/hr

C_5: $F_1C_{51} = F_5C_{55} + F_7C_{57}$
$F_7C_{57} = 20960.94642 - 0.00000 = 20960.94642$ kg/hr

C_6+: $F_1C_{61} = F_5C_{65} + F_7C_{67}$
$F_7C_{67} = 17816.80446 - 0.00000 = 17816.80446$ kg/hr
Total mass flow rate of the distillate:

$F_7 = F_7C_{17} + F_7C_{27} + F_7C_{37} + F_7C_{47} + F_7C_{57} + F_7C_{67}$

$F_7 = 761.93040 + 1802.64139 + 52402.36605 + 41921.89284 + 20960.94642 + 17816.80446$ kg/hr = 135666.58156 kg/hr

Component Mass fraction in bottom:

C_1 mass fraction: $\frac{761.93040}{135666.58156} = 0.00562$

C_2 mass fraction: $\frac{1802.64139}{135666.58156} = 0.01329$

C_3 mass fraction: $\frac{52402.36605}{135666.58156} = 0.38626$

C_4 mass fraction: $\frac{41921.89284}{135666.58156} = 0.30901$

C_5 mass fraction: $\frac{20960.94642}{135666.58156} = 0.15450$

C_6 mass fraction: $\frac{17816.80446}{135666.58156} = 0.13133$

Table 5: Calculated Mass Fractions and Mole Fractions for the De-ethanizer Column

Components	**Mass Fractions**			**Mole Fractions**		
	S-101	**S-102**	**S-201**	**S-101**	**S-102**	**S-201**
He	0.00010	0.00011	0.00000	0.00047	0.00050	0.00000
N_2	0.06000	0.06891	0.00000	0.04067	0.04262	0.00000
C_1	0.72700	0.83417	0.00562	0.86090	0.90111	0.01889
C_2	0.08600	0.09680	0.01329	0.05432	0.05578	0.02384
C_3	0.05000	0.00000	0.38626	0.02154	0.00000	0.47266
C_4	0.04000	0.00000	0.30901	0.01307	0.00000	0.28685
C_5	0.02000	0.00000	0.15450	0.00527	0.00000	0.11553
C_6+	0.01700	0.00000	0.13133	0.00375	0.00000	0.08223
Total	1.00010	1.00000	1.00000	1.00000	1.00000	1.00000

Table 6: Calculated Mass Flow rate and Mole Flow rate for the De-ethanizer Column

Component	**Mass Flow Rate (kg/hr)**			**Molar Flow Rate (kmol/hr)**		
	S-101	**S-102**	**S-201**	**S-101**	**S-102**	**S-201**
He	104.80473	104.80473	0.00000	26.20118	26.20118	0.00000
N_2	62882.8392	62882.8392	0.00000	2244.21268	2244.2126	0.00000
C_1	761930.402	761168.471	761.93040	47501.8954	47454.393	47.50190
C_2	90132.0695	88329.4281	1802.64139	2997.40837	2937.4602	59.94817
C_3	52402.3660	0.00000	52402.3660	1188.53178	0.00000	1188.53178
C_4	41921.8928	0.00000	41921.8928	721.29891	0.00000	721.29891
C_5	20960.9464	0.00000	20960.9464	290.51901	0.00000	290.51901

C_6+	17816.8044	0.00000	17816.8044	206.76343	0.00000	206.76343
Total	1048047.32	912485.543	135666.581	55176.8307	52662.267	2514.56319

Table 7: Calculated Percent Error for the De-ethanizer column

Balance	Input (Kg/hr)	Output (Kg/hr)	Error (%)
Overall	1048047.32068	1048152.12542	0.010
He	104.80473	104.80473	0.000
N2	62882.83924	62882.83924	0.000
C1	761930.40214	761930.40214	0.000
C2	90132.06958	90132.06958	0.000
C3	52402.36603	52402.36603	0.000
C4	41921.89283	41921.89283	0.000
C5	20960.94641	20960.94641	0.000
C6+	17816.80445	17816.80445	0.000

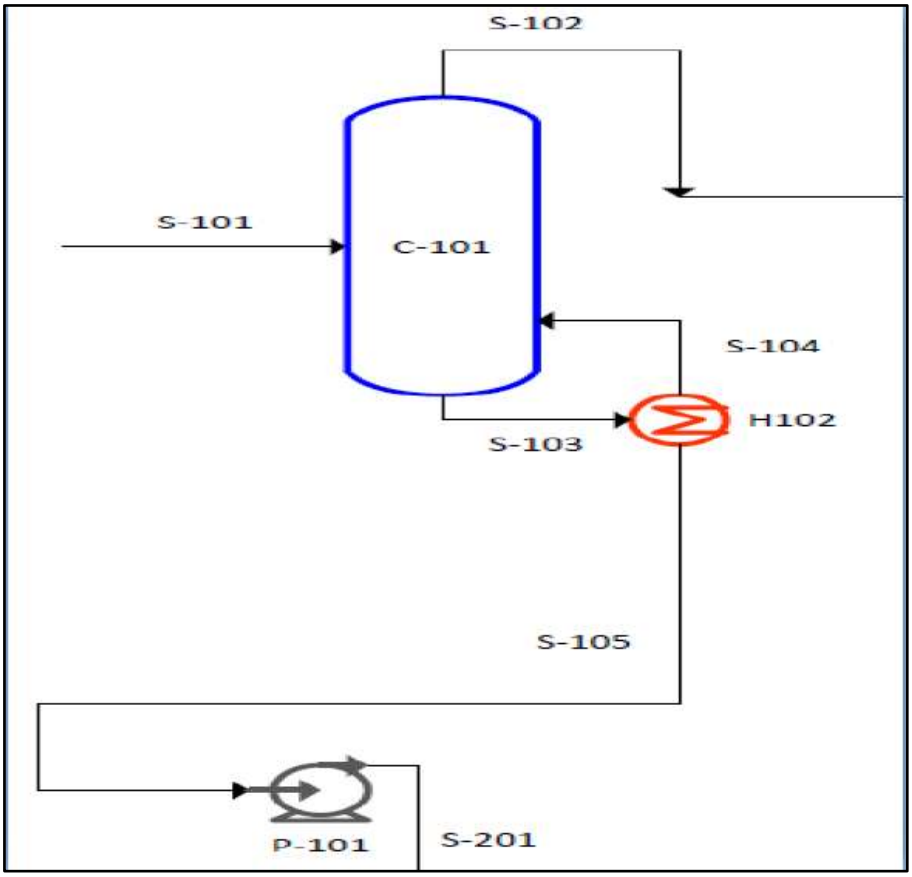

Figure 5: De-ethanizer Column

5.5 De-propanizer Column Unit Balance

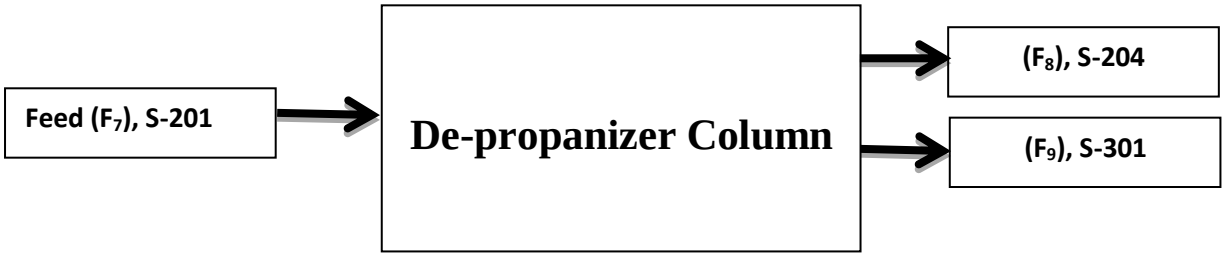

Figure 6: De-propanizer column unit balance block diagram

Components Material Balance in distillate:

C_1: $F_7C_{17} = F_8C_{18}$ = 761.93040 kg/hr

C_2: $F_7C_{27} = F_8C_{28}$ = 1802.64139 kg/hr

C_3: $0.999F_7C_{37} = F_8C_{38}$ = 0.999 (52402.36605) = 52349.96368 kg/hr

Total mass flow rate of the distillate:

$F_8 = F_8C_{18} + F_8C_{28} + F_8C_{38}$
F_8 = 761.93040 +1802.64139 + 52349.96368 kg/hr = 54914.53548 kg/hr

Component Mass fraction in distillate:

C_1 mass fraction: $\frac{761.93040}{54914.53548}$ = 0.01387

C_2 mass fraction: $\frac{1802.64139}{54914.53548}$ = 0.03283

C_3 mass fraction: $\frac{52349.96368}{54914.53548}$ = 0.95330

Components of material balance in bottom:

C_3: $F_7C_{37} = F_8C_{38} + F_9C_{39}$
F_9C_{39} = 52402.36605 – 52349.96368 = 52.402367 kg/hr

C_4: $F_7C_{47} = F_9C_{49}$ = 41921.89284 kg/hr

C_5: $F_7C_{57} = F_9C_{59}$ = 20960.94642 kg/hr

C_6+: $F_7C_{67} = F_9C_{69}$ = 17816.80446 kg/hr
Total mass flow rate of the bottom:

$F_9 = F_9C_{39} + F_9C_{49} + F_9C_{59} + F_9C_{69}$

F_9 = 52.402367 +41921.89284 + 20960.94642 + 17816.80446 = 80752.04608 kg/hr

Component Mass fraction in bottom:

C_3 mass fraction: $\frac{52.402367}{80752.04608}$ = 0.00065

C_4 mass fraction$\frac{41921.89284}{80752.04608}$: = 0.51914

C_5 mass fraction: $\frac{20960.94642}{80752.04608}$ = 0.25957

C_6 mass fraction: $\frac{17816.80446}{80752.04608}$ = 0.22064

Table 8: Calculated Mass Fractions and Mole Fractions for the De-propanizer Column

Component	**Mass Fraction**			**Mole Fraction**		
	S-201	**S-204**	**S-301**	**S-201**	**S-204**	**S-301**
He	0.00000	0.00000	0.00000	0.00000	0.00000	0.00000
N_2	0.00000	0.00000	0.00000	0.00000	0.00000	0.00000
C_1	0.00562	0.01387	0.00000	0.01889	0.03669	0.00000
C_2	0.01329	0.03283	0.00000	0.02384	0.04630	0.00000
C_3	0.38626	0.95330	0.00065	0.47266	0.91701	0.00097
C_4	0.30901	0.00000	0.51914	0.28685	0.00000	0.59134
C_5	0.15450	0.00000	0.25957	0.11553	0.00000	0.23818
C_6+	0.13133	0.00000	0.22064	0.08223	0.00000	0.16951
Total	1.00000	1.00000	1.00000	1.00000	1.00000	1.00000

Table 9: Calculated Mass Flow rate and Molar Flow rate for the De-propanizer Column

Component	Mass Flow Rate (kg/hr)			Molar Flow Rate (kmol/hr)		
	S-201	S-204	S-301	S-201	S-204	S-301
He	0.00000	0.00000	0.00000	0.00000	0.00000	0.00000
N_2	0.00000	0.00000	0.00000	0.00000	0.00000	0.00000
C_1	761.93040	761.93040	0.00000	47.50190	47.50190	0.00000
C_2	1802.64139	1802.64139	0.00000	59.94817	59.94817	0.00000
C_3	52402.36603	52349.96367	52.40237	1188.53178	1187.34324	1.18853
C_4	41921.89283	0.00000	41921.8928	721.29891	0.00000	721.29891
C_5	20960.94641	0.00000	20960.9464	290.51901	0.00000	290.51901
C_6+	17816.80445	0.00000	17816.8044	206.76343	0.00000	206.76343
Total	135666.5815	54914.53546	80752.0460	2514.56319	1294.79331	1219.76988

Table 10: Error Percentage for the De-propanizer Column

Balance	Input (Kg/hr)	Output (Kg/hr)	Error (%)
Overall	135666.58152	135666.58152	0.000
He	0.00000	0.00000	0.000
N_2	0.00000	0.00000	0.000
C_1	761.93040	761.93040	0.000
C_2	1802.64139	1802.64139	0.000
C_3	52402.36603	52402.36603	0.000
C_4	41921.89283	41921.89283	0.000
C_5	20960.94641	20960.94641	0.000
C_6+	17816.80445	17816.80445	0.000

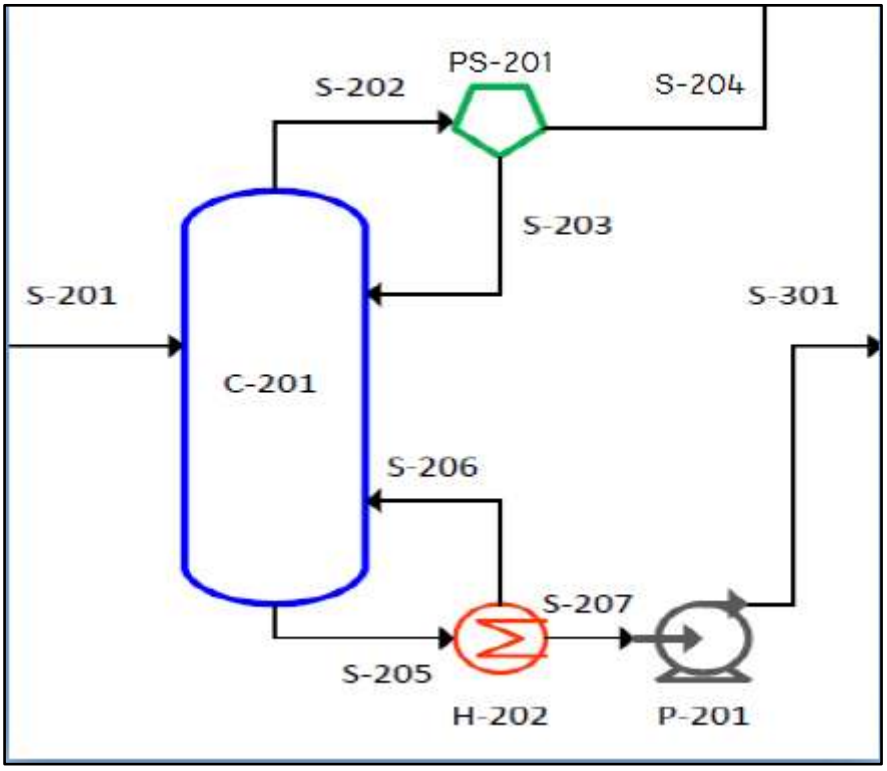

Figure 7: De-propanizer section

5.6 De-butanizer Column Unit Balance

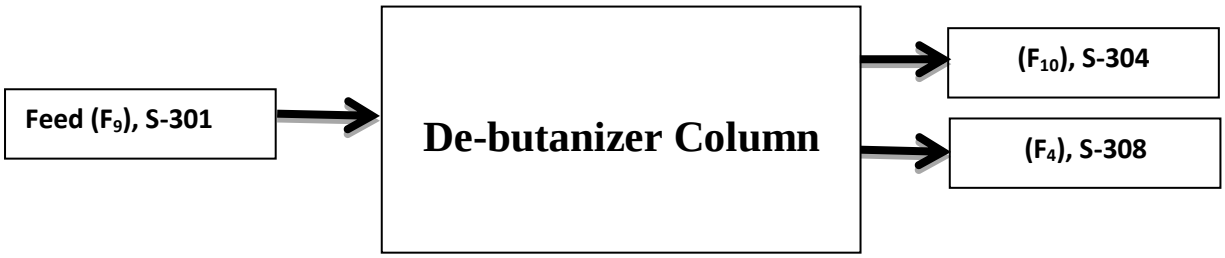

Figure 8: De-butanizer column unit balance block diagram

Components Material Balance in distillate:

C_3: $F_9C_{39} = F_{10}C_{310}$ = 52.40237 kg/hr

C_4: $F_9C_{49} = F_{10}C_{410} + F_4C_{44}$

$F_{10}C_{410} = F_9C_{49} - F_4C_{44}$ = 0.51914(80752.04608) – 0.006(39033.41976) = 41687.69232 kg/hr

Total mass flow rate of the distillate:

$F_{10} = F_{10}C_{310} + F_{10}C_{410}$
F_{10} = 52.40327 +41687.68232 = 41740.09469 kg/hr

Component Mass fraction in distillate:

C_3 mass fraction: $\frac{52.40327}{41740.09469} = 0.00125$

C_4 mass fraction: $\frac{41687.69232}{41740.09469} = 0.99874$

Components of material balance in bottom:

C_4: $F_9C_{44} = 0.006(39033.41976) = 234.20052$ kg/hr

C_5: $F_9C_{59} = F_4C_{54} = 0.537(39033.41976) = 20960.9464$ kg/hr

C_6: $F_9C_{69} = F_4C_{64} = 0.45645(39033.41976) = 17816.80446$ kg/hr

Table 11: Calculated Mass Fractions and Mole Fractions for the De-butanizer Column

Component	**Mass Fraction**			**Mole Fraction**		
	S-301	**S-304**	**S-308**	**S-301**	**S-304**	**S-308**
He	0.00000	0.00000	0.00000	0.00000	0.00000	0.00000
N_2	0.00000	0.00000	0.00000	0.00000	0.00000	0.00000
C_1	0.00000	0.00000	0.00000	0.00000	0.00000	0.00000
C_2	0.00000	0.00000	0.00000	0.00000	0.00000	0.00000
C_3	0.00065	0.00126	0.00000	0.00097	0.00165	0.00000
C_4	0.51914	0.99870	0.00600	0.59134	0.99831	0.00804
C_5	0.25957	0.00000	0.53700	0.23818	0.00000	0.57954
C_6+	0.22064	0.00005	0.45640	0.16951	0.00003	0.41242
Total	1.00000	1.00000	0.99940	1.00000	1.00000	1.00000

Table 12: Calculated Mass Flow Rate and Mole Flow Rate for the De-butanizer Column

Component	Mass Flow Rate (kg/hr)			Molar Flow Rate (kmol/hr)		
	S-301	S-304	S-308	S-301	S-304	S-308
He	0.00000	0.00000	0.00000	0.00000	0.00000	0.00000
N_2	0.00000	0.00000	0.00000	0.00000	0.00000	0.00000
C_1	0.00000	0.00000	0.00000	0.00000	0.00000	0.00000
C_2	0.00000	0.00000	0.00000	0.00000	0.00000	0.00000
C_3	52.40237	52.40237	0.00000	1.18853	1.18853	0.00000
C_4	41921.89283	41687.6923	234.20052	721.29891	717.26931	4.02960
C_5	20960.94641	0.00000	20960.9464	290.51901	0.00000	290.51901
C_6+	17816.80445	1.95167	17814.8527	206.76343	0.02265	206.74078
Total	80752.04606	41742.0463	39033.4197	1219.76988	718.48049	501.28939

Table 13: Error Percentage for the De-butanizer Column

Balance	Input (Kg/hr)	Output (Kg/hr)	Error (%)
Overall	80752.04606	80775.46611	0.029
He	0.00000	0.00000	0.000
N_2	0.00000	0.00000	0.000
C_1	0.00000	0.00000	0.000
C_2	0.00000	0.00000	0.000
C_3	52.40237	52.40237	0.000
C_4	41921.89283	41921.89283	0.000
C_5	20960.94641	20960.94641	0.000
C_{6+}	17816.80445	17816.80445	0.000

De-butanizer Efficiency = $\frac{Mass\ flow\ rate\ of\ C_4\ in\ the\ distillate}{Mass\ flow\ rate\ of\ C_4\ in\ the\ feed} \times 100\%$

$= \frac{41687.69232}{41921.89283} \times 100\ \% = 99.44\ \%$

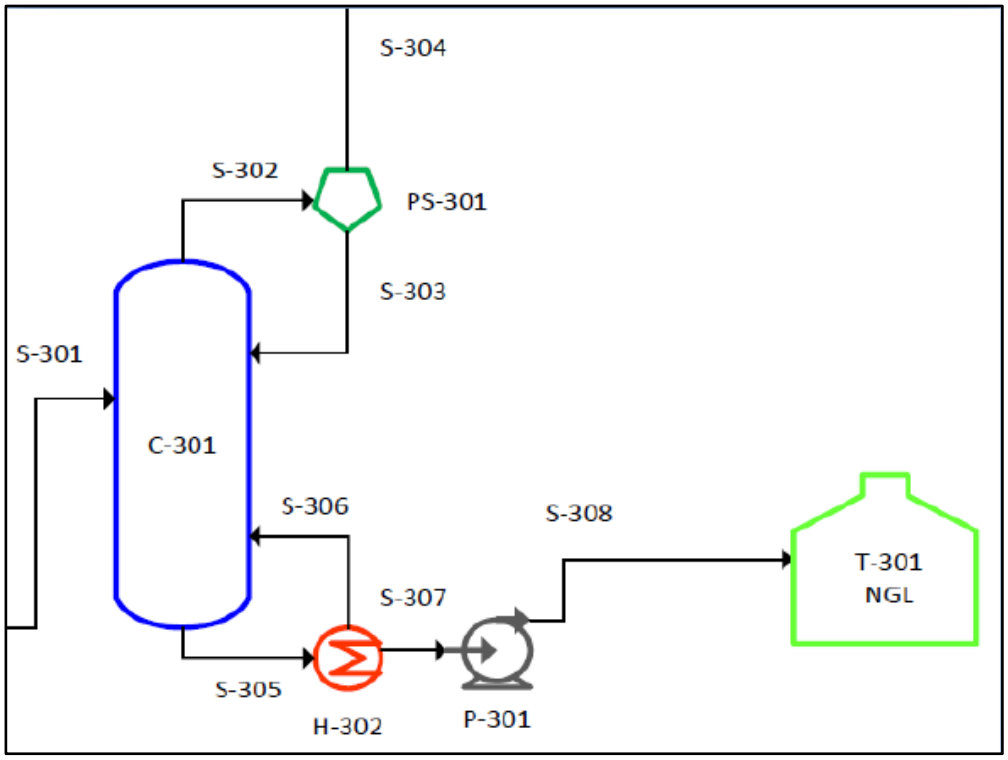

Figure 9: De-butanizer Section

5.7 Nitrogen Rejection Section

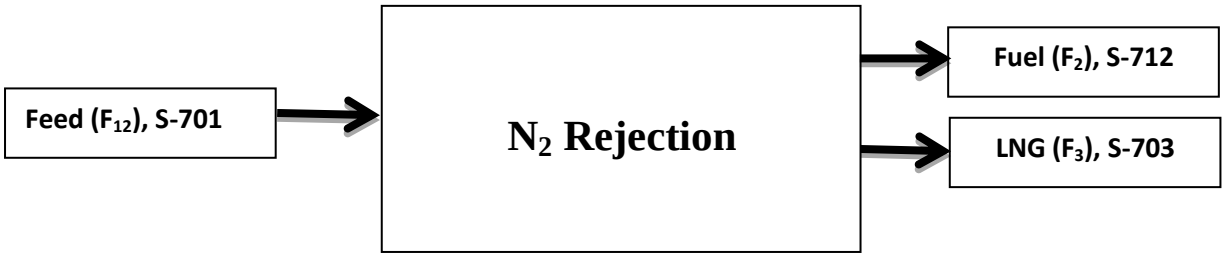

Figure 10: N_2 rejection column unit balance block diagram

Components Material Balance:

Overall: $F_{12} = F_2 + F_3$

$F_{12} = 158244.6705 + 850769.23077 = 1009013.901$ kg/hr

C_1: $F_{12}C_{112} = F_2C_{12} + F_3C_{13}$

$F_2C_{12} = 0.56762(158244.6705) + 0.79(850769.23077)$

$C_{12} = 0.755124$

C_2: $F_{12}C_{112} = F_2C_{22} + F_3C_{23}$

$F_2C_{22} = 0.0319447(158244.6705) + 0.1(850769.23077)$

$C_{22} = 0.08932668$

C_3: $F_{12}C_{321} = F_2C_{32} + F_3C_{33}$

$(1009013.901)C_{32} = 0.035(158244.6705) + 0.055(850769.23077)$

$C_{32} = 0.0518634$

C_4: $F_1C_{412} = F_3C_{43}$

$(1009013.901)C_{412} = 0.049(158244.6705)$

$C_{412} = 0.041315$

N_2: $F_{12}N_{12} = F_2N_2 + F_3N_3$

$(1009013.901)N_{12} = 0.36477(158244.6705) + 0.006(850769.23077)$

$N_{12} = 0.06227$

He: $F_1H_1 = F_2H_2$

$(1009013.901)H_1 = 0.0006623(158244.6705)$

$H_1 = 0.0001038$

Table 14: Calculated Mass Fractions and Mole Fractions for N_2 Rejection section

Component	**Mass Fractions**			**Mole Fractions**		
	S-701	**S-712**	**S-703**	**S-701**	**S-712**	**S-703**
He	0.00010	0.00066	0.00000	0.00048	0.00328	0.00000
N_2	0.06231	0.36512	0.00600	0.04105	0.25829	0.00390
C_1	0.75503	0.56762	0.79000	0.86880	0.70144	0.89741
C_2	0.08932	0.03195	0.10000	0.05482	0.02106	0.06059
C_3	0.05193	0.03545	0.05500	0.02174	0.01594	0.02273
C_4	0.04131	0.00000	0.04900	0.01312	0.00000	0.01536
C_5	0.00000	0.00000	0.00000	0.00000	0.00000	0.00000
C_6+	0.00000	0.00000	0.00000	0.00000	0.00000	0.00000
Total	1.00000	1.00080	1.00000	1.00000	1.00000	1.00000

Table 15: Calculated Mass Flow Rates and Mole Flow Rates for N_2 Rejection section

Component	Mass Flow Rates			Mole Flow Rates		
	S-701	S-712	S-703	S-701	S-712	S-703
He	104.80473	104.80473	0.00000	26.20118	26.20118	0.00000
N_2	62882.83930	57778.22391	5104.61538	2244.21268	2062.03511	182.17757
C_1	761930.4021	89822.70983	672107.6923	47501.89540	5599.91957	41901.9758
C_2	90132.06958	5055.14650	85076.92308	2997.40837	168.11262	2829.29575
C_3	52402.37164	5610.06395	46792.30769	1188.53190	127.24119	1061.29072
C_4	41687.69231	0.00000	41687.69231	717.26931	0.00000	717.26931
C_5	0.00000	0.00000	0.00000	0.00000	0.00000	0.00000
C_6+	0.00000	0.00000	0.00000	0.00000	0.00000	0.00000
Total	1009140.179	158244.6701	850769.2307	54675.51884	7983.50967	46692.0091

Table 16: Error Percentage for the Nitrogen Rejection section

Balance	Input (Kg/hr)	Output (Kg/hr)	Error (%)
Overall	1009140.1797	1009013.9009	0.01251
He	104.80473	104.80473	0.00000
N2	62882.83930	62882.83930	0.00000
C1	761930.40214	761930.40214	0.00000
C2	90132.06958	90132.06958	0.00000
C3	52402.37164	52402.37164	0.00000
C4	41687.69231	41687.69231	0.00000
C5	0.00000	0.00000	0.00000
C6+	0.00000	0.00000	0.00000

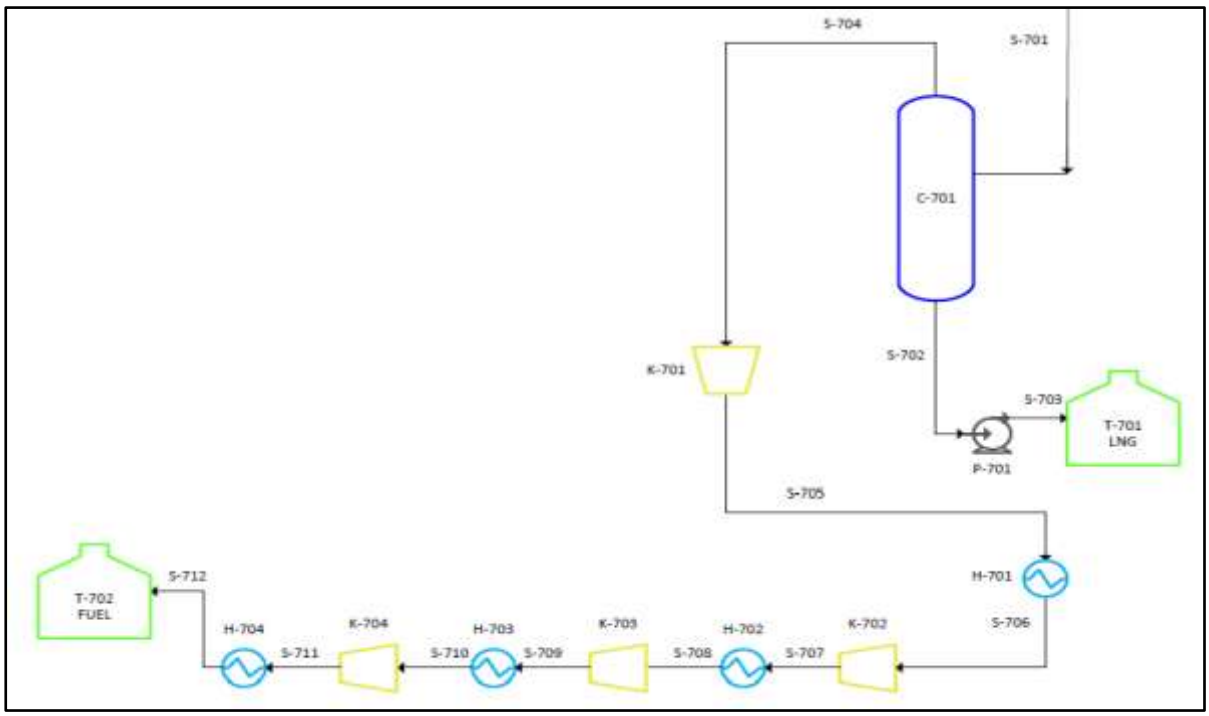

Figure 11: Nitrogen Rejection Section

RESULT & DISCUSSION

The molar flow rate and composition of the four streams are already calculated. In this section, the inlet and outlet streams are compared to check the calculated material balances.

Figure 12: Mixing section unit balance block diagram

The material balance was checked using the mixing section. Inlet flow rates and outlet flow rates were found to be equal with a percentage error of 0.0002%. The total flow rates, and components flow rates for each section were calculated, and the percentage error between inlet and outlet is given in the tables. The values show high accuracy of calculations, with very small errors. These errors might be due to some of the assumptions mentioned earlier. Approximations and rounding off significant figures can also slightly affect the results. However, practically, these errors can be neglected.

6.1 Overall Material Balance

Inlet:

$F_5 + F_8 + F_{10} = 912485.54389 + 54914.53546 + 41742.04635 = 1009142.1257$ kg/hr

Outlet:

1009140.17970 kg/hr

The two values approximately match, with a percentage error of:

$$\% \text{ Error} = \frac{(inlet - outlet)}{inlet} \times 100\ \%$$

$$= \frac{1009142.12570 - 1009140.17970}{1009142.12570} \times 100\%$$

$$= 0.00019\ \%$$

Table 17: Calculated Mass Fractions and Mole Fractions for the Mixing Section

Component	**Mass Fractions**			**Mole Fractions**
	S-102	**S-204**	**S-304**	**S-401**
He	0.00011	0.00000	0.00000	0.00010
N_2	0.06891	0.00000	0.00000	0.06231
C_1	0.83417	0.01387	0.00000	0.75503
C_2	0.09680	0.03283	0.00000	0.08932
C_3	0.00000	0.95330	0.00126	0.05193
C_4	0.00000	0.00000	0.99870	0.04131
C_5	0.00000	0.00000	0.00000	0.00000
C_6+	0.00000	0.00000	0.00005	0.00000
Total	1.00000	1.00000	1.00000	1.00000

Table 18: Calculated Mass Flow Rates and Mole Flow Rates for the Mixing Section

Component	Mass Flow rate			Mole Flow rate
	S-102	S-204	S-304	S-401
He	104.80473	0.00000	0.00000	104.80473
N_2	62882.83924	0.00000	0.00000	62882.83930
C_1	761168.47173	761.93040	0.00000	761930.40214
C_2	88329.42819	1802.64139	0.00000	90132.06958
C_3	0.00000	52349.96367	52.40237	52402.37164
C_4	0.00000	0.00000	41687.69231	41687.69231
C_5	0.00000	0.00000	0.00000	0.00000
C_6+	0.00000	0.00000	1.95167	0.00000
Total	912485.54389	54914.53546	41742.04635	1009140.17970

Table 19: Error percentage for the Mixing Section

Balance	Input (Kg/hr)	Output (Kg/hr)	Error (%)
Overall	1009142.1257	1009140.1797	0.00019
He	104.80473	104.80473	0.00000
N_2	62882.83924	62882.83930	0.00000
C_1	761930.40214	761930.40214	0.00000
C_2	90132.06958	90132.06958	0.00000
C_3	52402.36603	52402.37164	0.00001
C_4	41687.69231	41687.69231	0.00000
C_5	0.00000	0.00000	0.00000
C_6+	1.95167	0.00000	100.00000

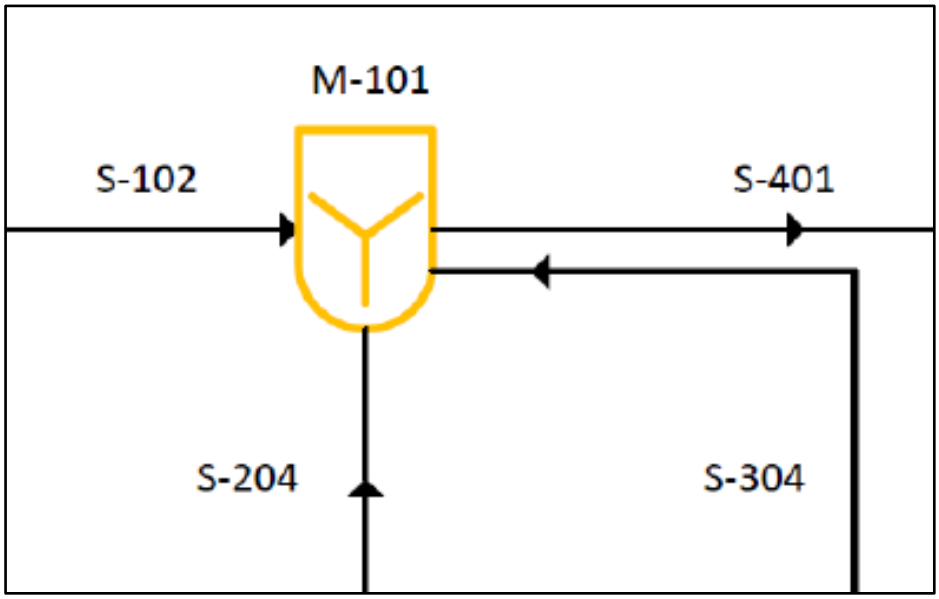

Figure 13: Mixing Section diagram

CONCLUSION

A world class Rich LNG plant is to be designed to produce 7.9 million ton per year to meet the increasing demand on natural gas around the world. The AP-X technology ranked number one in a comparison that was conducted between different available technologies and was chosen to be used in the plant.

Material balance calculations conducted to find the amount of feed necessary to produce the desired production rate and to calculate the different types and amount of utility needed to run the process. At each step and for every stream, the error percentage calculated. Almost all the streams gave no error or very minor percentages, and as expected, for each stream input was equal to output since there are no reactions.

Actually designing a complete plant that meets the expectations is not a straight forward one step, it is a process that is developed step by step as can be seen and explained in this report. Just like material balance calculations helped to realize that one of the columns initially placed in the fractionation section is dispensable, another energy balance calculation approach will help in realizing that amount of utility required can be reduced using heat integration.

REFERENCES

[1] *Material Balance Process. (n.d.).* Retrieved on December 15, 2015, from Resources: *http://www.ce.utexas.edu/bmb/resources/mass.html.*

[2] Shukri, T and Wheeler, F. (2004). LNG Technology Selection. Retrieved on May 5, 2016 from:http://www.fwc.com/publications/tech_papers/files/TariqLNG.pdf.

[3] V. Rivera, A. Aduku and O. Harris. (2008). Evaluation of LNG Technologies, May 2012, pp. 25-27.

International Conference on Petroleum Engineering 2016 (ICPE-2016)
Bangladesh University of Engineering & Technology (BUET)
Dhaka-1000, Bangladesh

ICPE (2016-042)

A Comparative Study of Modern Natural Gas Liquefaction Technology for Optimization of LNG Plant Efficiency

Mohammad Shahedul Hossain [1,*], Jumman Al Jawad [1]
[1] Department of Petroleum & Mining Engineering,
Shahjalal University of Science & Technology, Sylhet-3114, BANGLADESH

ABSTRACT

This paper deals with comparison of modern liquefaction technologies in midsize to large LNG plant projects to evaluate the most optimal natural gas liquefaction technology under different particular conditions, also to find out the major parameters to be considered before choosing appropriate liquefaction process. And research findings suggest a strategy for effective natural gas liquefaction process design. The research focuses on prevailing liquefaction technologies for LNG plant, which includes propane pre-cooled Mixed Refrigerant (AP-C_3MR), ConocoPhillips optimized Cascade process, AP-X technology and Dual Mixed Refrigerant (DMR) liquefaction technology. These technologies, as well as advantages and disadvantages of each, are analyzed very precisely. Throughout this paper we considered production capacity, cost per ton, required number of units and process efficiency as the major parameters based on which this comparative study was constructed. The results replicate comparative details of modern natural gas liquefaction technology and effect of different processes under different desired outcome, such as production rate, cost per ton, return on investment, plant efficiency etc. In fact this paper will overcome one of the key challenges of drawing a concise discussion on the prospective utilizations and management of the most logical liquefaction technology for meeting the desired LNG project goal.

Keywords: LNG liquefaction, DMR, AP-C_3MR, AP-X, N_2 cooling section, Cascade process

INTRODUCTION

Development of LNG technology has responded to growing LNG demand with new innovation in liquefaction technology. There are a number of LNG liquefaction technologies that are now in commercial use, such as: AP-C_3MR, AP-X, Air products & Chemical Inc. (APCI), Dual Cycle Refrigeration, Cascade (Triple Cycle Refrigeration), SMR, Shell DMR, Linde MFC process etc. Each of which is being used in various plants in the world depending on the plant criteria. These criteria include the capacity per train, market demand, environmental impact, safety issues, economics, plant size, reputation and proven records.

* Corresponding Author address
E-mail address: shahedulhossain@gmail.com

1.1 Background

Midsize LNG plants producing from 0.25-2.0 mta are being promoted as the way to monetize smaller stranded gas reserves at reduced cost. While the LNG industry trends in past years have been toward larger plants, it is important to note that a significant number of the operating base load LNG plants are in the capacity range of the midsize LNG market. Coil-wound heat exchangers (CWHE) in these midsize operating plants have demonstrated high reliability, operability, turndown stability and productivity for more than 40 years [1].

More LNG is produced using Air Products' MCR mixed refrigerant liquefaction processes than any other process in the world. And for good reason the LNG industry recognizes that liquefaction processes based on mixed refrigerants are the most efficient one. In addition, they have proven to be reliable, flexible, and easy to operate. To meet specific liquefaction requirements, we also can see several variations on modern LNG process, including dual mixed-refrigerant processes and the patented AP-X system used in the industry's largest LNG trains [1].

As of January 2016, global nominal liquefaction capacity totaled 301.5 MTPA, an increase from 291 MTPA at the end of 2014. Processes marketed by Air Products account for roughly 80% of installed plants: the AP-C_3MR process holds the greatest share at 49%, followed by the AP-X (16%) and AP-C_3MR/ Split MR (15%) processes.

Several under-construction projects have also selected MCR mixed refrigerant liquefaction processes. For instance, Cameron LNG and Yamal LNG will utilize the AP-C_3MR process, while Cove Point, Freeport LNG, Gorgon LNG, Ichthys LNG, and MLNG T9 will use the AP-C_3MR/ Split MR process. PFLNG 1 will use the AP-N process. Combined, these projects account for 76.2 MTPA (54%) of the 141.5 MTPA of capacity under construction as of January 2016. The large-scale AP-X process has thus far been used exclusively in Qatari projects.

However Conoco Phillips Optimized Cascade process will see strong growth with thirteen trains (57.2 MTPA of capacity) under construction using the process as of January 2016. As a result of its suitability to dry gas, the process has been the top choice for coal-bed methane (CBM) projects in Australia as well as some projects in the US, given their connection to the dry gas grid [5].

Other and increasingly smaller-scale processes make up a limited portion of existing and under-construction capacity but may see an increase in market share going forward. In North America, multiple projects have been proposed based on small-scale modular liquefaction processes. The use of these processes would allow developers to begin constructing liquefaction trains offsite, which may help to reduce costs [1].

AP-C_3MR Process

This technology has been leading the LNG process technologies for more than 30 years with its designs that were considered as the industry standard. Being used in almost 90% of the liquefaction industry, it is considered to be the optimum LNG technology to be used depending on the owner preferences and design basis. It is considered as the workhouse of the LNG industry for it has proven to be consistent, reliable, flexible and most importantly efficient. Since it is one of the original and longest used processes, it is responsible for the major proportion of the world's LNG production capacity producing from 1-5 mtpy of LNG per train [2].

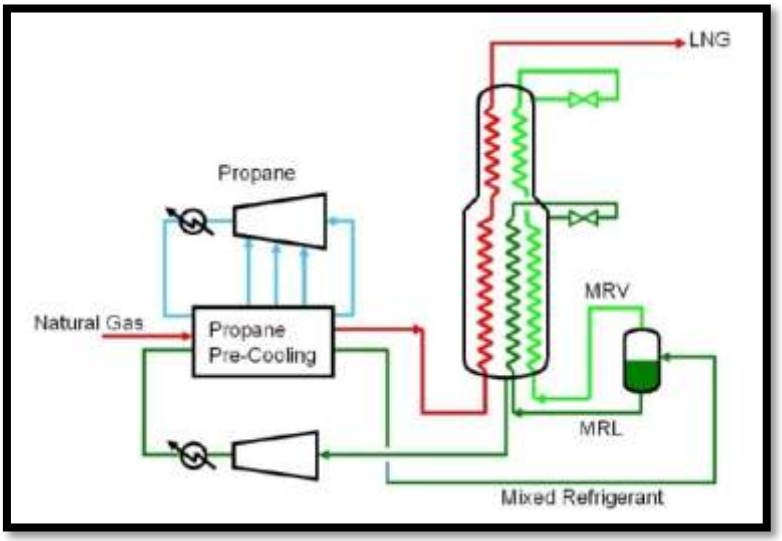

Figure 1: Air Products AP-C3MR™ LNG Process

A simple process flow diagram of the C3MR process is presented in Figure 1. The C3MR technology is mainly made up of two cooling cycles. The first cooling or refrigerant cycle is called the pre-cooling cycle and uses propane as a pure component. The second cycle is the sub-cooling and it uses a mixed refrigerant made up of methane, ethane, propane and nitrogen [2].

Depending on requirements, precooled mixed refrigerant processes, such as the propane precooled mixed refrigerant (AP-C3MR), provide an option that enhances efficiency while reducing the overall size of critical equipment. The Coil-wound heat exchanger (CWHE) can be fully modularized to minimize fieldwork. In fact mixed refrigerant process cycles with coil wound heat exchangers benefit from years of experience and know-how gained in the LNG industry [3].

The pre-cooling cycle consists of a series of three or four heat exchangers to precool the natural gas at three pressure stages, low, medium and high pressure. This is to allow the natural gas to be cooled to a certain initial temperature (-40^{o}C) before most of the cooling is achieved in the second cycle. It is also to cool and partially liquefy the mixed refrigerant which will be separated into vapor and liquid streams to be used to sub-cool and liquefy the process stream to -160°C in the mixed refrigerant or sub-cooling cycle. That takes place in a spiral wound exchanger known as the Main Cryogenic Heat Exchanger MCHE [4]. The main disadvantage for the C3MR process is its high equipment cost resulting from the use of the wound exchanger as well as the propane exchangers [4].

Conoco-Phillips Optimized Cascade Process

One of the global leaders in liquefied natural gas (LNG) is ConocoPhillips. Spanning more than five decades of LNG innovation, ConocoPhillips dependably develops main advances, from building the first LNG transporter for international trade to building one of the first effective commercial liquefaction facilities.

Nowadays, ConocoPhillips successfully operates facilities in Kenai, Alaska and Darwin, Australia, and has licensed its proprietary LNG liquefaction process to operators in different continents [5].

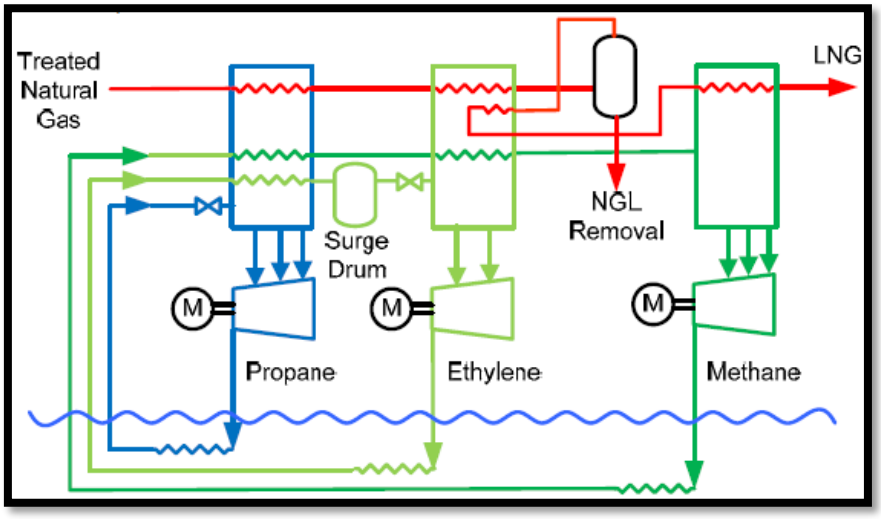

Figure 2: Optimized Cascade LNG Process

Using numerous of single components in separate refrigeration loops can achieve higher efficiency due to matching the cooling curve of the natural gas. This is the theory of the cascade process, which reaches the temperature necessary to liquefy the natural gas by cascading single component refrigerants in series [5]. By using propane, ethylene and methane as refrigerants with each one contained in its own closed loop system and supplies refrigeration at a discrete temperature level, the treated gas is chilled to about –260^{o}F in colder heat exchangers after it is treated to remove contaminants []. As any refrigeration process, increasing the number of refrigeration stages or utilizing a huge number of refrigerants may increase the efficiency. However, this improved efficiency requires an increase in equipment items, greater operating complexity, a potential impact on reliability and definitely higher capital cost [6].

AP-X Process

In recent years, a process with larger train capacities had to be developed to meet the increasing demand on liquefied natural gas. This process is the AP-X process and is suitable for train sizes greater than 6 million tpy and will increase the single train capacity to 7-10 million tpy.

Modern technology has been able to integrate successfully the liquefaction process design and the mechanical design of coil-wound heat exchangers (CWHE) to achieve performance and reliability unmatched in the LNG industry [1].

The AP-X process is basically a modification of the C3MR process. That is, it uses three cooling cycles instead of two. Simple process flow diagram of the AP-X process is presented in Figure 3. The addition of the third cycle which is the nitrogen sub-cooling loop placed after the wound heat exchanger, increases the efficiency and capacity of the process. This third cycle that is used to sub-cool the LNG reduces the duty of the MR system or the second cycle by reducing the amount of work done by the wound heat exchanger, permitting the production to increase to more than 80%.

Just like the C3MR process, the first cycle uses propane to pre-cool the LNG to an approximate temperature of -30°C, while the second uses a mixed refrigerant containing methane, ethane, propane and nitrogen to cool and liquefy the feed to exit the MCHE at -120°C. The third loop consists of two compressors to compress the pure nitrogen and then cool it by the two water-cooled heat exchangers [1]. It also contains the nitrogen expander that supplies the cold gaseous nitrogen for the final sub-cooling of the LNG. The reason that more cooling is done in the final loop, is that the nitrogen is able to cool to much lower temperatures than the mixed refrigerant. This also reduces the amount of mixed refrigerant used in the second cycle [1,5].

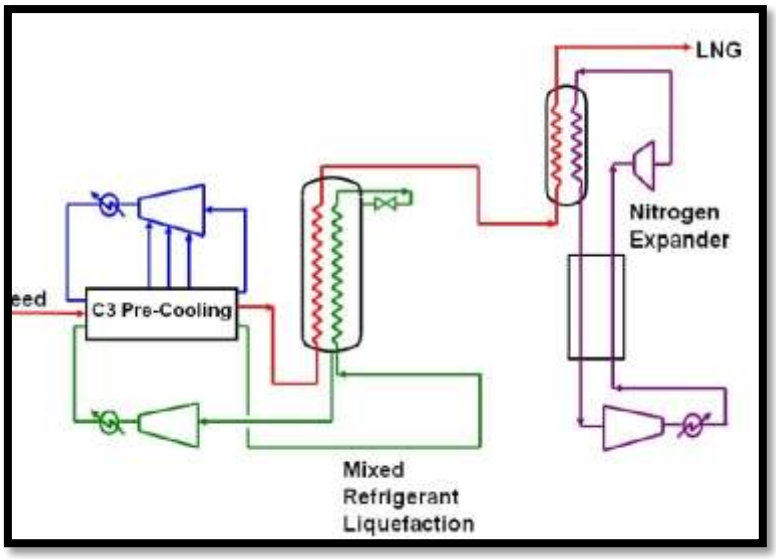

Figure 3: Air Products AP-X™ LNG Process

The simple modifications that were added to the C3MR resulted in a process that did not only increase the capacity of the LNG production with its high efficiency, but also reduced the capital cost per unit of LNG significantly. The main disadvantage of the AP-X process is the same as the C3MR, which is the equipment cost that lies in the amount of work performed by the compressors and the cost of the spiral wound heat exchanger [5].

The AP-X process uses both gas expander and fluid boiling cycles to their best advantage to achieve high efficiency and low cost.

Dual Mixed Refrigerant (DMR)

In countries that have various climate changes over the year, using a single component refrigerant in the pre-cooling cycle can impose some limitations on the process. Therefore, the DMR process has been developed to use a mixed refrigerant of a 50/50 molar basis composition of ethane/propane for pre-cooling to overcome these limitations. The advantage in this step is that the composition of the pre-cooling mixed refrigerant MR, which is heavier than the mixed refrigerant used for liquefaction or sub-cooling, can be adjusted depending on the temperature seasonal changes which cannot be done in

the traditional C3MR pre-cooling. However, in places like Qatar, temperatures and climate vary less, so using propane in the pre-cooling step using C3MR or AP-X makes more sense [7].

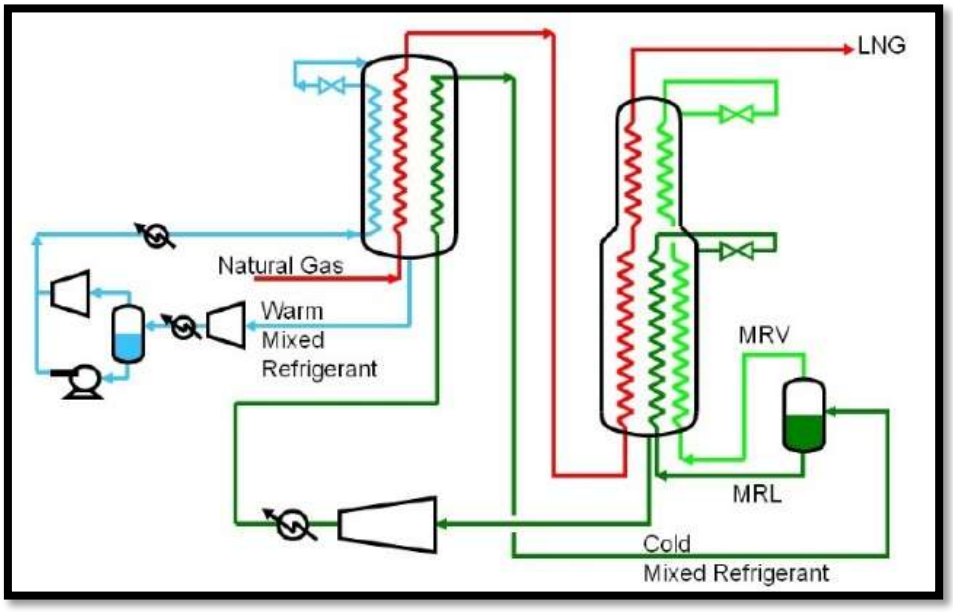

Figure 4: Air Products AP-DMR™ LNG Process

The natural gas feed stream is cooled via two MR stages in series. The first stage cools it to approximately -50°C while the second cools it to LNG at -160°C. The advantage of the two MR systems in series is that it presents a more flexible approach in selecting the pre-cooling temperature and a further optimal selection of compressors and drivers with certain feeds or ambient conditions. The DMR process production lies in the range of 2-4.5 million tpy and provides high thermal efficiency. Still, it has a great equipment cost, in addition to the complexity and multiple refrigerant handling [7,8].

Comparison of Discussed Liquefaction Technologies

The overall objective is to choose a proven process that should maximize the return on investment to the LNG owner. The following are some general considerations and guidelines to be followed to be able to answer the question asked earlier. First thing to be taken into consideration is the efficiency of the selected process. Low efficiency does not only result in a waste of resources and an increase in emissions, but from an economic view, it is a lost opportunity to produce and sell more LNG. Figure 5 represents a comparison between some of the most used technologies (including the four technologies discussed in this paper) thermodynamic efficiencies on a relative bases. AP-X, C3MR and DMR processes hold the first place with a thermodynamic efficiency of 100%, followed by Cascade, SMR and the N2 process.

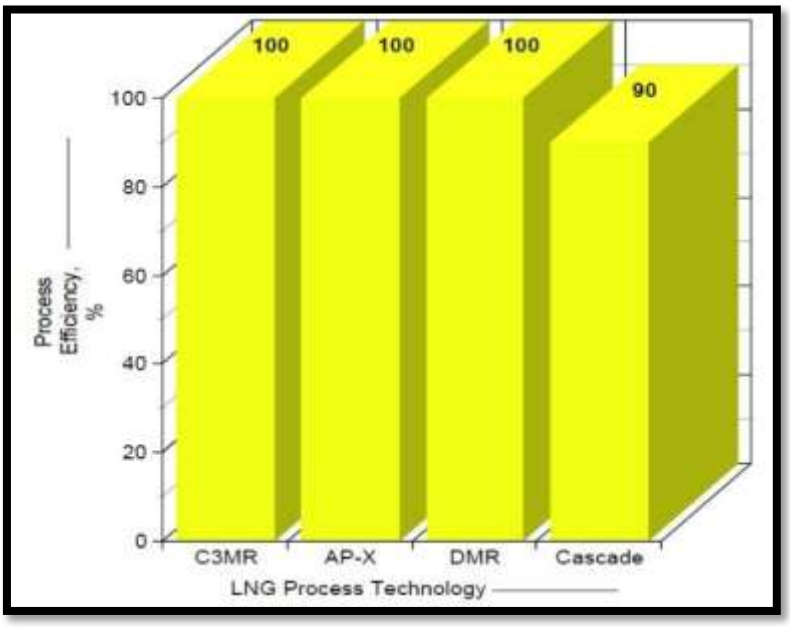

Figure 5: LNG Process Cycle Efficiency comparison
(LNG production per unit power)

Higher efficiencies will always make the process seem more economically attractive, since the resulting capacity will always justify the cost just as presented in Table 1 [4].

Table 1: Process Cost per Ton

Process	**Cost per ton ($)**	**Max capacity (MTPA)**
C3MR	12.93	4.80
Conoco	20.15	5.00
APX	19.20	7.80
DMR	17.50	4.50

It also should be taken into consideration that there will always be some compromises between additional capital cost and improved efficiency even after the process is selected. Therefore, the second factor to look at is the processing capacity [7]. The following figure shows the most applicable process choices for a given capacity.

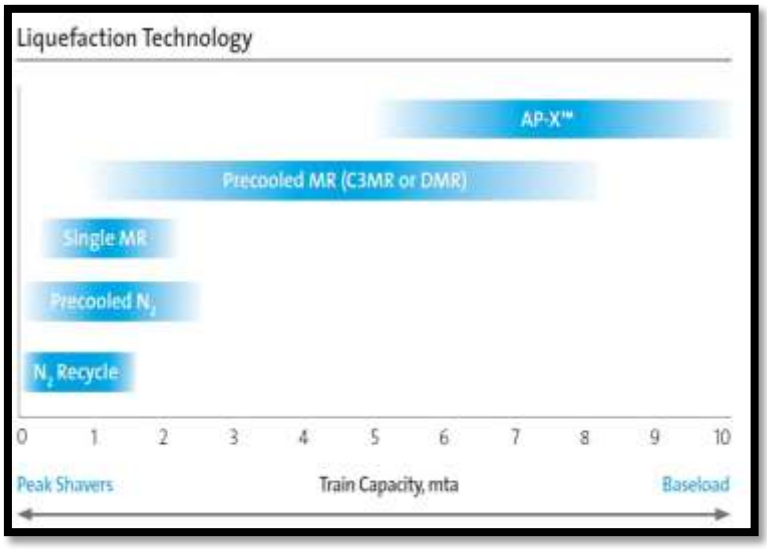

Figure 6: Liquefaction technology train capacity comparison, (mta)

Finally, operability and reliability are also two things that should be carefully considered by the LNG project developer while selecting the right process, due to the fact they directly affect the revenue stream.

RESULT & DISCUSSION

To select one of the four technologies mentioned above, and based on the main criteria discussed earlier, the following table shows the comparison between the technologies using rankings from 1-4, where:

1 – Poor; **2** – Good; **3** – Very good; **4** – Excellent

Since the capacity has a higher priority, its ranking is doubled. The objective is to produce with maximum capacity in million ton per annum. A technology that does not satisfy this objective cannot be selected. Table shows the results of the comparison [4].

Table 2: Technology Selection Criteria based on major parameters

Technology	**Criteria**				**Total**
	Capacity × 2	**No. of Units**	**Efficiency**	**Cost per ton**	
C_3MR	3	3	4	3	16
AP-X	4	3	4	2	17
DMR	2	4	4	4	16
Cascade	2	1	3	1	9

Based on the above comparison, AP-X technology is selected to be implemented in our plant. According to the above comparison, AP-X has the highest ranking compared to the other technologies. It is also the only technology that can meet our proposed target objective of production capacity. Its efficiency is about 100% and the cost is not much higher than the other technologies given that it is an improved version of C3MR technology. It has one unit in addition to C3MR, with a higher production rate.

CONCLUSION

Choosing the optimum LNG liquefaction technology is the first most important decision in the design process, since it has a large impact on the overall profitability of an LNG project. To provide the proper selection, four main LNG technologies have been discussed with a complete design basis and information on the criteria being used by LNG owners. The four technologies that were discussed are the most widely used in industry, and these are the C3MR, AP-X, DMR and the Cascade process. Based on a comparison made between these technologies taking into consideration the plant criteria, AP-X technology is the one chosen to be applied in our plant. It is the technology which meets our proposed target objective of having high capacity of the LNG production with high efficiency. The efficiency is one of the main criteria of which our choice was built upon, due to the fact that poor efficiency means more emissions and less opportunity to sell and produce more LNG. The other criteria should also be considered carefully because it represents an important factor to accomplish the LNG project successfully.

REFERENCES

[1] *The World Leader in LNG Technology, Equipment and Services*. 1st ed.: 12-23, Allentown, PA: Air Products and Chemicals, Inc., 2016.

[2] Shukri, T and Wheeler, F. (2004). LNG Technology Selection. Retrieved on May 5, 2016 from:http://www.fwc.com/publications/tech_papers/files/TariqLNG.pdf.

[3] McKeever, Jack, Mark Pillarella, and Ron Bower, "An Ever Evolving Technology", *LNG Industry*, Spring Issue 2008.

[4] V. Rivera, A. Aduku and O. Harris. (2008). Evaluation of LNG Technologies, May 2012, pp. 25-27.

[5] Liquefied Natural Gas. (2009). Retrieved on May 5, 2016, ConocoPhillips LNG Brochure, http://lnglicensing.conocophillips.com/EN/Documents/ConocoPhillipsLNG_Brochure.pdf .

[6] Cascade LNG Process. (n.d.). Retrieved on May 15, 2016 from ConocoPhillips: http://lnglicensing.conocophillips.com/EN/publications/documents/quartercentury.pdf .

[7] Roberts, Mark Julian, Rakesh Agrawal, "Dual Mixed Refrigerant Cycle for Gas Liquefaction", US Patent 6,119,479, 19 September 2000.

[8] Gauberthier, J., Paradowski, H., "New Trends for Future LNG Units", Session II, Paper 6, The 9th International Conference and Exhibition on Liquefied Natural Gas (LNG9), Nice, France, 17-20 October, 1989.

International Conference on Petroleum Engineering 2016 (ICPE-2016)
Bangladesh University of Engineering & Technology (BUET)
Dhaka-1000, Bangladesh

ICPE (2016-055)

Mathematical Analysis of Effects on the Electrostatic Double Layer of Nanoscale Surfaces in Microfluidic Channels

D. E. Aston [1], C. Berven[2], B. Williams[3], A. Basu*[4]
[1]Department of Chemical and Materials Engineering, PO Box 441021, University of Idaho, Moscow, ID, USA 83844-1021
[2]Department of Physics, University of Idaho, Moscow, ID, USA 83844-0903
[3]Department of Agricultural and Biological Engineering, University of Idaho, Moscow, ID, USA 83844-0904
[4]Department of Chemical and Biological Engineering, South Dakota School of Mines and Technology, Rapid City, SD, USA 57701-3995

ABSTRACT

The effects of microfluidics on the electrostatic double layer (EDL) of a nano-structured electrode are investigated through numerical modeling. The parameters of interest are the height and spacing of nanostructures, specifically, nanowire and "nanopillar" pairs rising from an idealized sensor substrate perpendicular to the fluid flow.

Keywords: Electroosmotic velocity, Electrostatic Double Layer, Zeta Potential

INTRODUCTION

Micro-fluidic studies with respect to anionic adsorption, has been partially illustrated with numerical solutions [1]. The detection and quantification of anions such as arsenates are conducted with spectroscopic, chromatographic and electrochemical techniques [2, 3, 4]. However, these techniques are often complex and expensive by nature. Recent advances in nanoscience technologies are being utilized for efficient environmental monitoring techniques. Using existing techniques, TRACEDETECT, INC is developing a sensor that will be applicable to measuring arsenic levels in drinking water [5]. The objective of our proposal is to design a portable sensor that will assist in on-site monitoring of anions in a contaminant plume in both surface and ground water.

This proposed work will prioritize the detection of pure anionic species. Microchannels with nanomaterial electrodes have recently been made and tested for flow. The next step is to reproduce and optimize the design for fluid flow. The proof-of-concept for characterization and optimization of sensor will include determination of background sensor signal from the nanoelectrode under flowing conditions without

analyte. This background signal or noise will be effectively summed with 'observed' potential changes (due to anion concentration) under steady state conditions. The hypothesis is that relative changes in nanoelectrode potentials are functions of analyte concentrations and are correlated with anion sorption to the nanowires. Chemical modification of nanowire networks will be through metal particle deposition and conjugation with binding molecules.

Biological instruments often rely on electrokinetic mechanisms for fluid transport in channel dimensions of 10-100 microns [6]. Microfluidic systems offer the ability to maintain laminar fluid diffusion interfaces ideal for the production of stable concentration gradients [7]. These materials function within the framework of a quantum confined induced phenomena without the need for expensive apparatus. They are used for biological and chemical sensors [8] and molecularly gated switches [9]. In pursuance to its versatile properties, metallic [8], semi-conducting [10], dielectric [11] and perovskite nanowires [12] have been synthesized for specific purposes. The charged substrate of the sensor used for quantification of anions is composed of a mat of nanowires coated with gold nanoparticles and occupies a specific amount of space in the channel. Nanowires are attractive nanomaterials for a variety of reasons; however, it is their versatility that makes them attractive from technical standpoint [13]. Such sensors are also associated with electrically driven separation techniques such as DNA isolation [14]. Materials being utilized for fabrication of sensors include carbon nanotubes , polypyrrole nanowires and gallium nitride nano wires.

The carbon nanotubes due to their unique structures and electrical properties have attracted considerable attention as nanowires. The electronic structures of the nanotubes are either metallic or semi-conducting, depending on their chirality and diameter [15]. The intrinsic properties of nanotubes such as conductivity and reactivity can be controlled by interaction with oxygen and thus there is considerable possibility of developing nano-electronic devices as semiconductors [16]. Polypyrrole nanowires have also been utilized to successfully detect nitrate ions from a lower concentration limit of 1.52*10-6 M solution [17]. The conductive polymer nanowires inherit unique electrical properties for sensing applications [18]. These materials display excellent performances as two terminal resistive sensors using Conducting Polymer Nanowires Electrode Junction (CPENJ) arrays and are correlated to high sensitivity and fast responses in detecting HCL and NH3 gases [19]. Due to rapid response and easier handling methods, anion selective electrodes are being commercially used for selective analytical purposes [20, 21].

Gallium nitride (as anion sensitive electrode) based high–electron mobility transistor devices have been developed for a variety of electronic applications. The induced polarity of the gallium to nitrogen bond causes an electron defective nature of the gallium atoms that promotes enhanced reactivity with electron-enriched bases [22].

THEORY

When the charged species such as arsenic (electron-enriched base) adsorbs to the capillary wall, it alters the surface charge on the wall and therefore zeta potential [23]. Initially, total number of adsorption sites on the capillary wall remains vacant without ionic interactions. However, after a fully developed flow is attained at steady state conditions, the zeta potential varies with respect to time interval. This is attributed

to increase in adsorption of the charged species on the capillary wall before the substrate is fully saturated with the 'adsorbed ions'. Thus if the saturated site distribution across the entire substrate is uniform, the electro osmotic velocity (u) of the fluid at steady state condition is expressed as [23]:

$$\mu = \frac{-\varepsilon \xi E}{4\pi\mu} \qquad (1)$$

Where ε is the dielectric constant of medium, μ is the viscosity of the buffer solution, ξ is the zeta potential at the substrate and E is the external electric field. The forces of importance in typical electro osmotic flow include flow inertia, pressure forces, viscous stresses and Lorentz body force acting on the charges inside the electric double layer (λ). If the height of channel (h) is relatively larger than the thickness of double layer, the flow through the medium is defined by a plug flow region [24]. Otherwise, flow is dominated by two regions defined as electro-osmotic flow within diffusion layer and pressure driven flow in bulk phase, as shown in Figure 1.

In addition, the application of an external electric field confirms the hypothesis that fluid flow through a channel of micron dimensions (in width and/or height) is influenced by interfacial effects such as electric double layer (EDL) [25]. The double layer is formed due to the interaction of the ionized solution with the positive based charges on nanowires such as the gallium nitride based semiconductor [2].

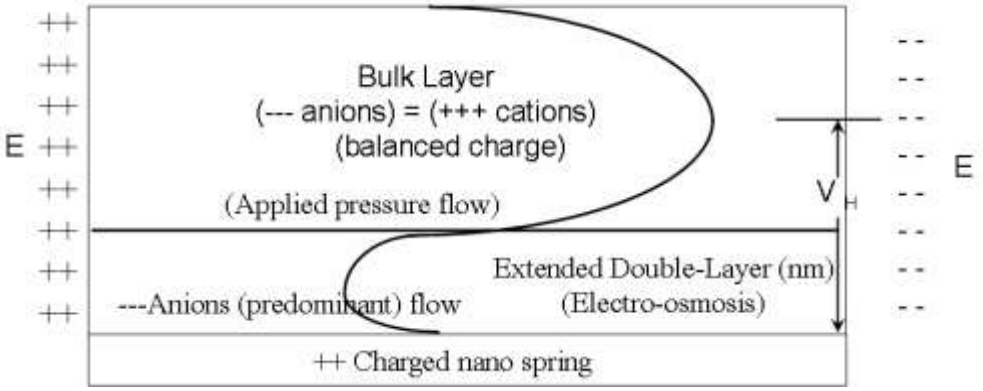

Figure 1: Schematic diagram of microfluidic sensor with mixed electro-osmotic and pressure-driven flow regimes.

The anions in the bulk phase migrate toward the positively charged wall forming a Stern layer of typical thickness of one ionic diameter. Immediately above the Stern layer, the diffuse Helmholtz layer consisting of a high density of anions is formed [26]. The variation of the ion density is correlated to the Boltzman distribution which is consistent with a mathematical derivation based on statistical and mechanical considerations. If the potential shift generated is based on the selective adsorption of the anions inside the

double layer, the sensitivity factor of detection of the contaminant will depend on ΔV_H value. At steady state conditions, it is displayed that this value is proportional to the surface excess charge due to adsorption of anions and inversely proportional to the double layer capacitance. The sensitivity factor will vary for different ranges of anion concentrations. Hence it will be important to investigate the effect of sensitivity factor at appropriate ranges (ppm-ppb) of anion concentrations in a plume.

The sensitivity factor is dependent on the intrinsic coefficients associated with a sensor. They include capacitance (C_H), number of adsorption sites (Γ), surface coverage (θ) and energy of interaction (f). These are some of the parameters that affect the sensitivity of the potentiometric response. The effect of multi-component anions on the overall potentiometric response is the ultimate objective (beyond this project) for development of such a sensor. This will be accomplished by determining potential shifts of the single components in bulk phase and then monitoring the responses as a function of concentrations of multi-component ions at steady state. The interaction of several species with respect to a charged substrate are related with factors such as the total number of charged sites, influent concentrations and specific adsorption coefficients of the species [27]. The double layer is expressed as [28]:

$$\lambda = \left[\frac{\varepsilon\varepsilon_0 k_b T}{8\pi n_0 e^2 z^2} \right]^{0.5} \qquad (2)$$

z is the valence of the ion. The thickness of the double layer is determined experimentally by locating the layer in bulk phase where the electric force acting on the anion is counterbalanced by the viscous drag of the charged particle. It will be followed by utilizing a set of empirical equations to locate the double layer [29]. However, determination of anionic concentration by this technique (utilizing above equation) is time consuming and hence the estimated values of the effective double layer are initially used for calibrating the sensor.

The calibration of the sensor (both experimental and numerical methods) is essential to correlate the potentiometric response as a function of the anionic concentration in the bulk phase. To investigate the mechanism of potentiometric response as a function of the analyte concentration in the bulk phase, it is significant that the surface of gallium nitride nanowires interacts selectively with the charged anions. Lalonde and coworkers [30] have developed a technique for growing nanoparticles with average diameters in range of 1.5-2.5nm on the surface of nanowires. This technique has been successfully used to coat nanowires with Ni, Pt and Au particles. Under such conditions, the observed response is due to the adsorption of the specific ions inside the double layer. This is also suggested by Chaniotakis and coworkers [2]. The model based on the potentiometric response is due to adsorption mechanism based on fixed site ion exchange theory. It has been recommended that the sensitivity of the substrate of the semiconductor can be expressed as [2]:

$$\frac{d\Delta V_H}{d\ln|n_0|} = \frac{zF\Gamma}{\left[\frac{1}{\theta(1-\theta)} + f + g\right]} C_H^{-1} \quad (3)$$

Where $g = \frac{z^2F^2\Gamma}{C_H RT}$, z is the charge, F is the faraday constant, R is the universal gas constant and T is the absolute temperature. f and θ are interaction coefficient and surface coverage respectively. At values of (f) below zero, the attractive forces between the nanowires and anions are dominant by nature [31]. The interaction parameter f, is also a function of surface coverage, θ [32]. The potentiometric response is also expressed as:

$$V_H = \frac{zF\Gamma}{\left[\frac{1}{\theta(1-\theta)} + f + \frac{z^2F^2\Gamma}{C_H RT}\right]} \ln n_0 \quad (4)$$

The response value is used to determine the anionic concentration n_0 and is compared with the values of n_0 obtained from equation 4. The discrepancy in the results is assessed for calibration purposes.

It is assumed that the activity of the ionic solution is equal to its concentration (n_0) in moles per m^3. In relation to effluent concentrations at ppb, the arrangement is reasonable, but in relation to incomplete disassociation of anions in bulk phase, correction factors have to be estimated. The potentiometric response ΔV_H, is the potential drop generated across the double layer. This response is essentially equal to the zeta potential (ζ) at the slip plane. The thickness of the stern layer is approximately equal to the radius of a hydrated ion, the present approach neglects the thickness and assumes zeta potential (ζ) is equal to wall potential [30]. The wall potential can often be considered to be approximately equal to the response ΔV_H. This is an assumption considered because it is impossible to determine the absolute surface potential at the wall. Though there will be electrodes attached to measure the surface potential, the mat is highly irregular.

It is highly recommended to initiate studies of variance of potentiometric responses in relation to the thickness of the mat. The effect of ratio of effective double layer to thickness of the mat will be monitored with respect to the potentiometric response of the sensor. Present studies at Department of Chemical Engineering of University of Idaho, indicate that wettability of the mat (a parameter that may be linked with potentiometric response) is dependent on its thickness. Numerical studies are required to interpret the effective double layer as either a sum of individual layers of each wire or the reciprocal of effective double layer is a sum of reciprocal values of individual double layers of each wire.

RESULTS AND DISCUSSIONS

Our modeling results have confirmed that with the application of an external electric field, fluid flow through a channel of micron dimensions (in width and/or height) is influenced by interfacial effects such as the EDL [1]. This is expected since the thickness of the EDL even in planar structures (i.e., geometrically simpler devices) would be in the range of nanometers or microns. It can be argued that when the EDL thickness—both at the surface of the nanomaterial-based ISE and the silica glass microchannel walls—are significantly smaller than the characteristic dimensions of the microchannel, the velocity profile may become independent of the cross sectional area of the channel. However, for the case of pressure-driven flow, as we will impose in our device on top of a constant electro-osmotic field, the parabolic flow profile and mean flow rate would be expected to depend on the cross sectional area of the microchannel. The thickness of the EDL scales varies only with □ under static or no-flow conditions. However, within the inner region of flow (within □ of the surface), the flow behavior of the liquid is dominated by movement of analyte under the effect of an external electric field. The velocity of the liquid associated with the inner region is defined as Helmholtz- Smoluchowski velocity and can be considered as a good approximation of the velocity profile near the wall [28]. When negatively charged species adsorb to the ISE, they will alter the surface charge on the substrate and the local zeta potential value. At initiation of the flow, adsorption sites on the ISE will be vacant with no ionic interactions. However, after attainment of fully developed flow and steady state conditions, a new value of the zeta potential is achieved. This is attributed to an increase in the adsorption of the charged species onto the capillary wall along with adsorption of ions onto the ISE. Under the new steady-state conditions, the saturated site distribution across the entire substrate is uniform.

The electro-osmotic velocity (equation 7), u_{eo}, of the fluid under steady flow conditions may be expressed as the Helmholtz-Smoluchowski velocity [23]:

$$u_{eo} = \frac{-\varepsilon \zeta E_x}{4\pi\eta} \tag{5}$$

where ε is the dielectric constant of medium, ζ is the potential at the slip plane of the substrate, and E_x is the applied external electric field. To further elucidate the relative changes in the EDL thickness at key points in our channel, we have introduced a normalized EDL thickness (equation 6), □*, that is the ratio of the EDL thickness at the top of one of the obstructions (e.g., nanowire) to the EDL thickness at the mid-point of the substrate surface (that is, the bare electrode material of the ISE underneath the selective nanomaterial of interest) between two identical obstructions:

$$\delta^* = \frac{\delta_{99_{top}}}{\delta_{99_{bottom}}} \tag{6}$$

The effective EDL thickness, δ_{99}, is the number of Debye lengths, □, from the wall where the electro-osmotic potential, ϕ, decays to 1% of its surface value [28]. The EDL thickness is typically in the nanometer range but can be much greater under very low ionic concentrations**.** This parameter is dependent on the net electrostatic attraction of the ions to the substrate; that is, increasing the electrostatic attraction will cause a significant decrease in EDL thickness and decreasing microfluidic impact on the

actual thickness of the EDL. Here, of course, there will also be a variable function of the fluid flow regime which will impact the effective EDL extent near the ISE.

The ratio □* is in essence a measure of the relative displacement of the double layer at the higher topographical points in the microchannel. The obstructions of the nanowires standing vertical from the surface provide some protection of the EDL at the substrate level from the depleting results of the fluid flow above it. Another physical interpretation of δ^* is to consider it as a dimensionless type of volumetric flow rate defect due to redistribution of fluid momentum within the EDL caused by the nanoscale obstructions. This similar qualitative understanding of the EDL redistribution phenomenon has been previously related to the total volumetric flow rate through the inclusion of combined pressure-driven/electro-osmotic function and a volumetric defect parameter describing an effective EDL displacement in microfluidics [25, 28].

Some anions are transiently bound to the surface due to electrostatic attraction. The remaining anions close to the positive substrate are in rapid thermal motion and form the EDL. If an electric field E_x is imposed in the system, these mobile ions will drift towards the driving anode. Thus, the effective EDL formation will be modified by the degree of retention of the anions and it will be the result of the balance of electrostatic and advective forces. Hence, applied velocity slips that incorporate EDL effects are imposed as boundary conditions on nanowires and substrate. In order to accommodate specific slip conditions for all surfaces, the Helmholtz-Smoluchowski velocity must be used in the analysis [28]. Table 1 provides the parameters used in the computations corresponding to expected operating conditions in our microfluidic device currently under test.

Table 1. Physical constants utilized in our modeling.

Operating Parameters	Numerical values
Height of microchannel	20 □m
Bulk flow rate as average velocity	0.03, 0.3, 3.0, 30, 300 (□m/s)
Density of fluid (ρ)	1 g/cm^3
Viscosity of fluid (η)	10^{-3} kg/m-s
Thickness of nanowire (d)	50 nm

Height of nanowire (*H*)	200 nm, 2 μm
External electric field (*E*)	-100 V/m
Zeta potentials (ζ_i, ζ_j)	-75 mV, +75 mV

Effect of Zeta Potential and Flow Rate on EDL

In order to begin an exploration of the effect of the electro-osmotic fluid behavior in the vicinity of a nanowire network or nanospring mat serving as an ISE, we have modeled the fluid flow over idealized, nanoscale obstructions (mimicking a 2D flow profile over vertical nanowire "pillars") and calculated the EDL thicknesses along this convoluted electrode surface as a function of the spacing between obstructions. In relation to EOF in microchannels, parameters such as Debye length, microchannel width and flow rate have been considered previously for parametric studies [25]. In relation to the scope of this work, the effect of flow rate, height of the obstruction, *e.g.*, nanowire, and their spacing have been selected for easy parametric analysis.

We have performed this analysis for nanowire spacing of 2, 30, 100, 200, 500 and 5000 nm at bulk fluid velocities of 0.3, 3.0 and 30 □m/s. Two extreme velocities (30 nm/s and 300 □m/s) are also used in the initial EDL modeling but are not of immediate interest to the application of a feasible microfluidic sensor for ionic detection. The EDL thickness of the substrate ($\delta_{99bottom}$) is determined to be insensitive to this range of flow rates outside of the influence of nanoscale obstructions to flow and is calculated as 270 nm, with a monovalent electrolyte concentration of 0.01 mM at 298 K. The static Debye length, □, under these conditions is 96.2 nm, where static δ_{99} = 443 nm.

The existence of an EDL at the substrate can be attributed to a competition between electrostatic attraction and thermal diffusion forces. The net attractive force at the substrate allows the capture of counter-ions and repulsion of co-ions from the lower boundary. The co-ions, under influence of the external electric field, move in the opposite direction of the average fluid flow in this scenario. Stronger ionic repulsions will result in a significant increase in $\delta_{99bottom}$. Thus, the EDL thickness is determined to be inversely related to the bulk flow rate and parameter $\delta_{99,}$ increases with increasing viscous forces for larger spacings, where the nano-obstructions do not interfere electrically (Fig. 4).

However, we note that for nanowire spacing of less than 500 nm, the repulsive co-ion effect is significantly reduced because of the countering effect of the nanowire surface potentials closing in on the fluid volume in the vicinity.

In general, the EDL at the top of the obstructions (that is, further into the center of the microchannel) is largely reduced in comparison to the EDL that is somewhat shielded between them at the substrate. This is supported by the monotonically decreasing □* values with increasing velocity of Fig. 2.

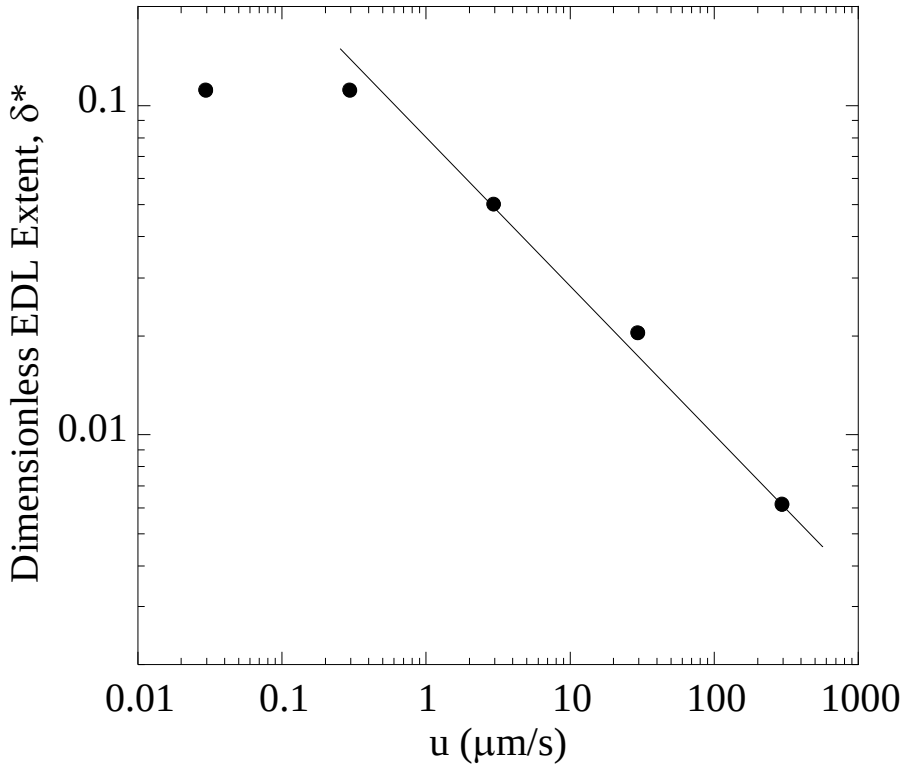

Figure 2: Relative EDL thickness profile as a function of microchannel fluid velocity (0.03, 0.3, 3, 30, 300 □m/s) with L_j = 100 nm, H = 200 nm, i.e., nanopillars. (Straight line for visual reference only.)

An average input velocity of 300 nm/s is low enough to approach that static double layer condition; however, the morphology of the charged surface is not uniform and the applied external electric field drives mobile charges in solution continuously, which can contribute to □$_{99bottom}$ being even more than ten times the value of □$_{99top}$. Furthermore, the highest velocity is impractical for microchannel experiments with the present particle imaging capabilities in our facilities. However, the data suggest, that even greater effects may still be imposed on the EDL redistribution within a nanowire network or a nanospring mat, if higher velocities can be attained. Further parametric studies reveal that the normalized EDL (□*) is inversely dependent on the aspect ratio (L_j/H), at velocities above 300 μm/s.

As expected, the value of □* approaches unity asymptotically for larger aspect ratio (Fig. 3), though the limit of □* for large spacing between nanowires will also be affected by the channel height and velocity.

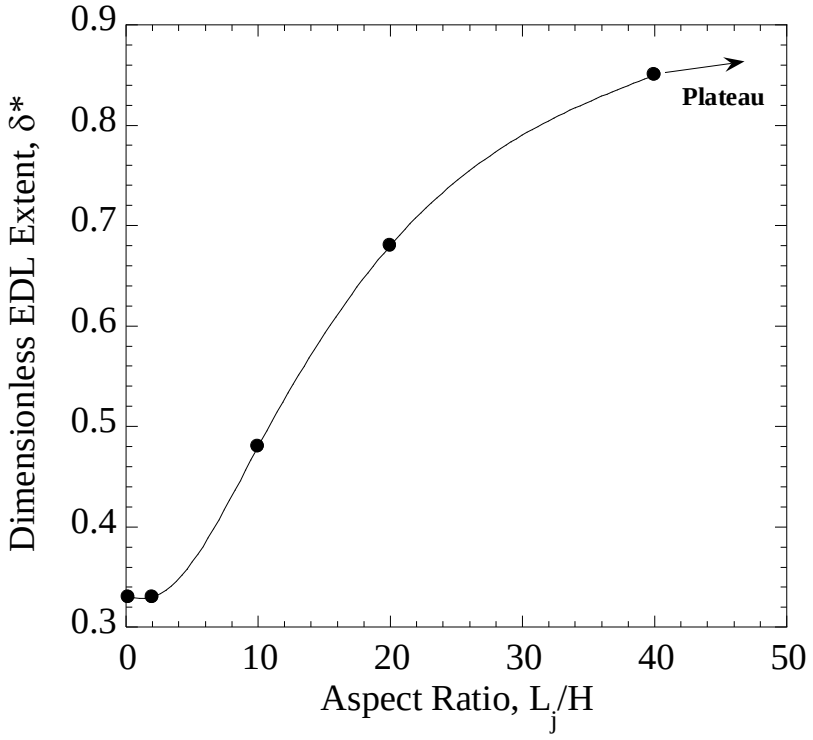

Figure 3: EDL thickness ratio for nanowires (H = 2 □m) as a functional of spacing-to-height aspect ratio at a velocity of 30 μm/s: cubic spline-fitted curve.

In the simulated case, with the nanowire being 10% of the microchannel height, the pressure-driven fluid flow will have a significant impact on □*, as is discussed below in further detail. In Fig. 3, the curve is more interesting for smaller spacing, where □* appears to have another limiting value as the nano-obstructions approach each other. This result may not be fully understood by a qualitative explanation of the combined effects of the microfluidic differences in the zone at the top of the nanowires and the fluid regime between the nanowires at the substrate. As the spacing becomes increasingly smaller, we observe □* decrease until the spacing is <400 nm. As the spacing decreases, the effective contribution of the bottom electrode potential (□$_j$) also decreases. The potential distributions are convoluted further by the direct impact of each nanowire's surface potential on the other. The very interesting result is that the EDLs at the top and bottom are changing at nearly the same rate for spacing between 400 nm and 4 □m, which is significantly larger than the EDL thicknesses under this microfluidic regime. In this "plateau" regime of intermediate spacing, the competition between pressure-driven microfluidics and the opposing zeta potentials is weaker than is observable for much smaller spacing.

Figure 4 shows that the EDL at the ISE substrate between the nanowires (□$_{99bottom}$) grows rapidly with spacing, regardless of the average velocity, because the electrostatics become the dominant phenomenon on the extent of the EDL both in the constricted region between nanowires (where the fluid medium becomes effectively stationary) and at their ends extending into the microchannel.

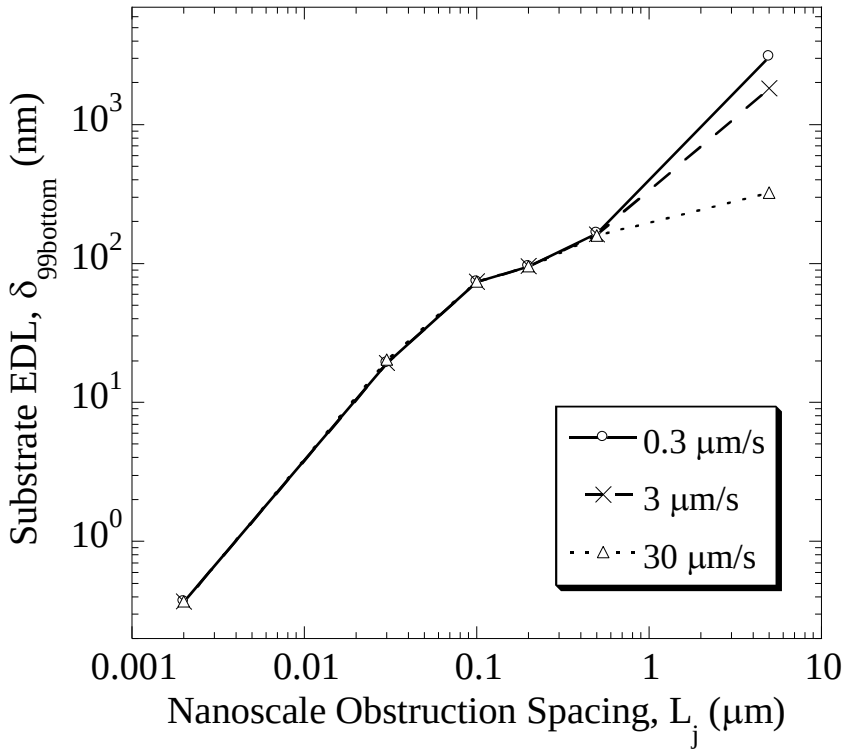

Figure 4: EDL thickness at the ISE substrate between the obstructions, □*99bottom* (□m), vs. spacing between two nanopillars (*H* = 200 nm).

The onset of this interesting intermediate regime begins at different spacing values, depending on the imposed microfluidic conditions, but is highly affected by the spacing than by the velocity parameter, when the spacing becomes of the order of the Debye length, viz., roughly □*99*. This phenomenon is consistent with observations of capillary systems subjected to axially varying electro-osmotic velocity [1]. While Fig. 4 displays only the nanopillar case for H = 200 nm, it is unnecessary to examine the taller nanowires (H = 2 □m) for the purposes of this study. It is sufficient to observe from equation 2 that the value of ζ_{ave} is higher for H = 2 □m than at 200 nm at the same spacing, L_j, and therefore the onset of the intermediate EDL network regime will begin at larger spacing values for taller nano-obstructions. By qualitative extension, the same argument is valid for thicker mats of fibrous nanomaterials that comprise the ISE. Furthermore, the decreasing trend in □*99bottom* with decreasing L_j cannot continue indefinitely, since the underlying substrate essentially disappears as the hypothetical ISE morphs into a new solid extended surface of the nanowire material, with uniform zeta potential □*i*, exhibiting the trivial flat plate behavior. Figure 4 plots also demonstrate that at an obstruction spacing range of .001-0.6 (approx) microns, the value of $\delta_{99bottom}$ is independent of pressure driven flow. In this range, the variation of

$\delta_{99_{bottom}}$ is directly proportional to the nano wire spacings. This is possibly linked to the dominance of diffusive and electrokinetic forces at inner flow zones. At steady state conditions, with increase in obstruction spacing and proportionate increase in diffusivity of ions, more anions are adsorbed on the positive charged substrate. This results in decrease of substrate potential and a corresponding increase of EDL thickness. At a critical value of approximately 0.6 micron spacing and above, the stream line bulk flow contours are more capable to transport the anions from the vicinity of the substrate. Thus at this 'critical value' and above, the bulk flow pattern is predominantly correlated to mitigation of adsorption of anions onto the substrate.

The EDL thickness at the end of the nanowire (δ_{99top}) is generally reduced to a larger extent than $\delta_{99bottom}$ by increasing fluid flow, which is in agreement with Fig. 2, resulting in the generally decreasing trends in δ. The plots for both nanopillar and nanowire scenarios are displayed in Fig. 5.

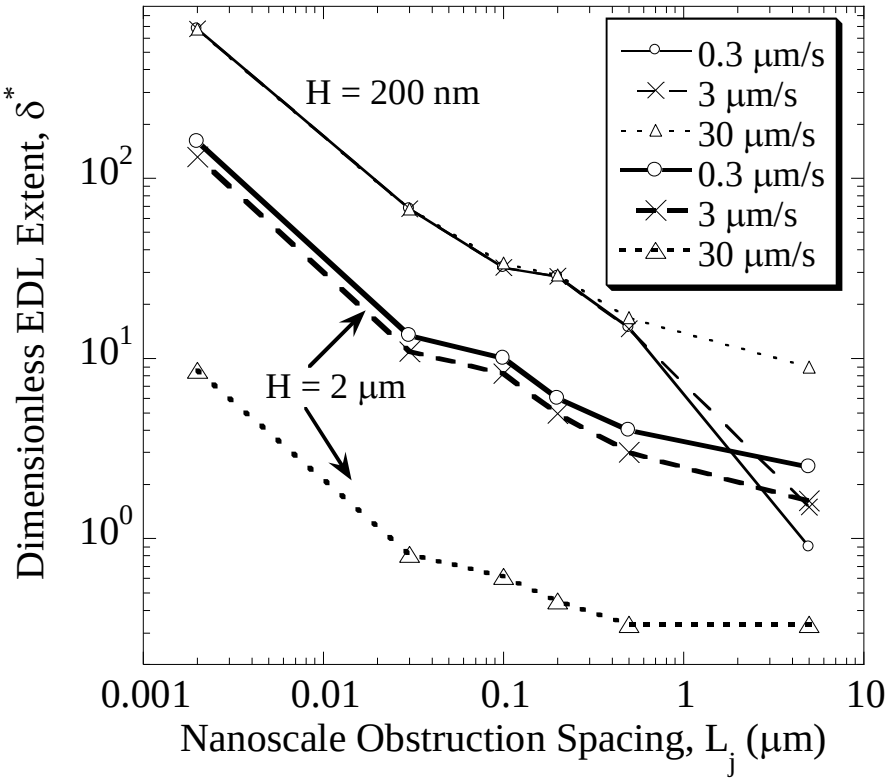

Figure 5: EDL ratio (δ^*) with respect to spacing for nanopillars (H = 200 nm) and nanowires (H = 2 μm).

The expected interplay between the flow obstruction height, H, and spacing, L_j, on the EDL thickness at the highest (δ_{99top}) and lowest ($\delta_{99bottom}$) points along the ISE contour is shown to be rather complex in behavior. The EDL of the substrate is drastically reduced between the nano-obstructions for small spacings due to the competing influences of oppositely charged surface potentials. The average zeta potential of the entire region grows more positive than the zeta potential of the substrate and results in

lower anion mobility within the localized EDL. Excess cations migrate toward the cathode and their net mobility is in the same direction as the bulk flow. This results in significant depletion of the EDL at the substrate.

The resulting EOF is diminished in correlation with increases in □*, which in Fig. 5 represents the redistribution of the EDL away from the substrate, thus thickening the EDL at the nanowires. At a bulk flow velocity of 30 □m/s, the value of □*, for example, is 0.33 for a corresponding parameters of H = 2 □m and L_j = 5 □m. By comparison, □* is 2.5 for a corresponding velocity of 0.3 □m/s, where □$_{99bottom}$, is 0.12 □m and H = 200 nm. Under an identical set of physical parameters for H = 200 nm (nanopillars), the thickness of this EDL was computed as 0.3 □m. The taller obstructions (nanowires) act as more of a barrier to perturbations of the EDL at the substrates and □$_{99}$ values are less sensitive to flow rates. However, ζ_{ave} values are significantly affected by longer nanowires than by the shorter nanopillars of the same specific spacing. Lower advective forces coupled with higher electrostatic interactions result in significant depletion of the EDL at the substrate and a corresponding increase in □*. Thus at nanopillar heights of 200 nm, the advective forces become insignificant.

Figure 5 also illustrates the EDL distribution with respect to bulk flow velocities. It can be observed that at nano pillar heights of 200nm, an increase in spacing of obstructions is directly proportional to increase in EDL thickness at the substrate. However, since the local stream line velocity at height of 200nm is extremely insignificant, diffusion dominated transport of anions is prevalent. It is apparent that at spacings of approximately 0.6 microns and above, an increase in bulk velocity, leads to diminished sorption of anions on substrate. Thus the substrate potential increases with higher velocities, which in turn leads to proportionate decrease of $\delta_{99bottom}$.

However, at heights of 2 microns, the stream line velocities have a significant effect on the EDL thicknesses at the 'peak' of the nanospring. Proportionate increase in stream line velocities, abet in transporting the anions from the plateau and this results in significant increase of surface potential at the top of the nano spring. Thus the EDL thickness at the top decreases significantly with proportionate increase of surface potential. At higher aspect ratios, the dispersion of anions to the substrate is limited by the advective transport. The effect is reflected by monitoring the value of $\delta_{99bottom}$.which denotes that it remains significantly unaffected with variation in flow rates.

The EDL at the substrate for both obstruction heights is relatively insensitive to velocities lower than 30 □m/s, where the determining factor for effective EDL profiles is nanowire spacing [1].

A complex variable to be investigated is the extent of the wettability of a real nanowire network or nanospring mat that makes up the ISE in our fabricated sensors. This will bear a direct impact on the measurement of the potentiometric response ϕ targeted for the analyte of interest. This wettability will be determined by a number of factors [1], including the morphologies of each nanostructure, such as the coiling of a nanospring, and on effective porosity of a nanosensor mat that consists of a random network of interwoven nanofibers, nanowires, or nanosprings. Secondly, for numerical simulations, the EDL thickness at both nanomaterial electrode and the microchannel sidewalls will affect each other at the edges, where the present study was a two-dimensional, semi-infinite construct. However, the variations of

the flow fields at the edges are not expected to result in large discrepancies between simulations and measurements when the typical microchannel width to height ratio dimension is greater than 10.

CONCLUSIONS

The changing dimensions of the ISE at the nanoscale have a tremendous impact on the redistributing of the EDL surrounding the network of nanomaterials the comprising the sensing electrode. These simulations display that very significant morphological effects on a convoluted EDL are possible when nanomaterials are distributed on a surface with geometric spacings that are of the same order of as the EDL thickness and lower. The effective Debye length, λ_{eff}, of a real nanowire or nanospring network will eventually be related to the dimensionless EDL thickness profile, ψ^*, which may ultimately be reduced to a ratio of the extreme EDL thicknesses within a designed mat of fibrous or other 1D nanomaterials. This demonstrates that the most significant fabrication parameter to experimental studies of ISE may in fact be the nanowire morphology as a lumped parameter, such as extrema and average values of ψ^*, rather than some fundamental characterization of nanospring or nanowire length and diameter, and the thickness of the matted nanomaterial that would result from laborious electron micrograph studies.

The next step to making a quantitative connection between the ISE sensitivity in modes of potentiometric detection, V_H, will be to determine, through experiments, the effect of complex nanowire networking on the simplified theoretical parameters ψ^* and λ_{eff} as functions of the fluid flow regime. The prospect of accomplishing this stage of experimental analysis is not trivial and will require significant efforts and innovations in the methodical approach of chemical sensor design. The very highly-convoluted surface morphology of silica nanospring networks will remain difficult to understand or model adequately until many incremental steps in simplified cases are better described. The future goal for directed chemical sensor electrode design will continue to be the development of more rigorous system-property relationships that can connect microfluidic behavior in nanoporous structures with morphology and detection response.

ACKNOWLEDGEMENT

The authors gratefully acknowledge support from the National Science Foundation (BES-0507921, EPS-0447689) for the initiation of the project.

REFERENCES

[1] Aston, D.E., Berven, C., Williams, B., and Basu, A., (2012). Mathematical Analysis of effects on electrostatic double layer of nano-scale surfaces in micro-fluidic channels, *Canadian Journal of Chemical Engineering*, vol 90. 1059-1065

[2] Chaniotakis, N., Alifragis, Y., Konstantinidis, G., and Georgokalis., A., (2001) Gallium nitride _based potentiometric anion sensor, *AnalyticalChemistry*, vol.76, No.18, 5552-5556

[3] Davenport, R.J., and Johnson, D.C., (1973) D.C. Voltammetric determination of nitrate and nitrite ions using a rotating cadmium disk electrode, *Analytical Chemistry*, 45, 1979-1980

[4] Casella, I.G., and Gatta, M., (2004) Electrochemical reduction of nitrate and nitrite and nitrite ions on a composite copper thallium electrode in alkaline solutions, *Journal of Electro-analytical Chemistry*, 568, 183-188.

[5] Trace Detect Inc., NIEH Grant No: R44ES012758, 06/2005-05/2007

[6] Herr, A.E., Molho, J.I., Santiago, J.G., Mungal, M.G., Kenny T.W. and Garguilo, M.G., (2000) Electroosmotic capillary flow with nonuniform zeta potential, Analytical Chemistry, vol.72, 1053-1057

[7] Bliss, E., and Li, D., (2005) Electrokinetic generation of temporally and spatially stable concentration gradients in microchannels, Journal of colloid and interface Science, vol.288, No.2, 606-618

[8] Goglio, G., Pignard, S., Radulescu, A., Piraux, L., Huynen, I., Vanhoenacker, D., and Vander Vorst., A., (1999) Microwave properties of metallic nanowires, *Applied Physics Letters*,vol.75, No.12, 1769-1772

[9] Huber, T.E., and Graf., M.J., (1999) Electronic transport in a three dimensional network of one dimensional Bismuth quantum wires, Physical Reveiew letters, 60, 168-180

[10] Seo, H.W., Bae, S.Y., Park, J., Yang, H., Park, K.S., and Kim., S., (2002) Strained gallium nitride nanowires, Journal of Chemical Physics, vol.116, No.21, 9492-9499

[11 Liang, C.H., Meng, G.W., Wang, G.Z., Wang, Y.W., Zhang, L.D., and Zhang, L.Y., (2001) Catalytic synthesis and photoluminescence of β –Ga2O3 nano wires, *Applied Physics Letters*, vol.78, No.21, 3202-3204

[12 Zhu, D., Zhu, H., and Zhang, Y., (2002) Hydrothermal synthesis of La Ba 0.5 MnO3 nanowires, *Applied Physics Letters* , vol. 80, No.9, 1634-1637

[13] McIlroy, D.N., Alkkhateeb., A., Zhang, D., Aston., D.E., Marcy, A., and Norton, M.G., (2004) nanospring formation – unexpected catalyst mediated growth, *Applied Physics Letters*, vol.16, 415-440

[14]Walters, L.C., Jacobson, S.C., Kroutchininia, N., Khandurina, J., Foote, R.S., and Ramsey., J.M., (1998) Microchip device for cell lysis, multiplex PCR amplification,and electrophoretic sizing, Analytical Chemistry, vol.70, 158-162

[15] Valentini, L., Cantalini, C., Armentano, I., Kenny, J.M., Lozzi, L., and Santucci, S., (2004) Highly sensitive and selective sensors based on carbon nanotubes thin films for molecular detection, 14th European conference on diamond, diamond like materials , carbon nanotubes, nitrides and silicon carbide, vol.12, Issues 4-8, April-August, 1301-1305

[16] Chico, L., Crespi, V.H., Benedict, L.X., Louie, S.G., and Cohen M.L., (1996) Pure carbon nanoscale devices: Nanotube hetero-junctions, *Physics Review Letters*, vol.76, 971-974

[17] Zhang, X., Wang, J.X., Wang, Z., and Wang, S.C., (2005) Improvement of amperometric sensor used for determination of nitrate with polypyrrole nanowires modified electrode, *Sensors*, vol.5, pp.580-593

[18] Alam, M. M., Wang, J., Guo, Y., Lee, S.P., and Tseng, H.R., (2005) Electrolyte-gated transistors based on conducting polymer nanowire junction arrays, Journal of Physical Chemistry B., 109, 12777-12784

[19] LaLonde, A., Norton, G., McIlroy, D., Zhang, D., Padmanabhan, R., Akhlateeb, A., Han, H., Lane, L., and Holman Z., (2005) Metal coatings on SiC Nanowires by plasma enhanced chemical vapor deposition, Journal of Material Resources, vol.20, No.3, 549-553

[20] Asghari, A., Amini, M.K., Mansour, H.R., Salavati-Niasari, M., and Rajabi, M., (2003) Nitrate-selective membrane electrode based on 2-hydroxyanil) acetylacetone lead(II) neutral carrier, *Analytical Science*, 19, pp.1121-1125

[21] Badea, M., Amine, A., Palleschi, G., Moscone, D., Volpe, G., and Curulli, A., (2001) *Journal of Electro-analytical Chemistry*, 509, pp.66-72

[22] Costales, A., Kandalam, A., Pendas, M., Blanco, M., Reico, J.M., and Pandey, R.,(2004) Journal of Physical Chemistry, 104, pp.4368-4370

[23] Shariff, K., and Ghosal S., (2004) Peak Tailings in electrophoresis due to alteration of the wall charge by adsorbed analytes A Aumerical simulations and asymptotic theory, *Analytica Chimica Acta*, vol.507, pp.87-93

[24] LaLonde, A., and Norton,G., (2005) Metal coatings on SiC nanowires by plasma enhanced chemical vapor deposition, Journal of Material Resources, vol.20, No.3, Materials Research Society.

[25] Yang, R., Fu, L.M., and Lin., Y.C., (2001) Electroosmotic flow in microchannels, Journal of colloid and interface science, vol.239, pp.98-105

[26] D. Shaw, *Charged interfaces*, Introduction to Colloid and surface chemistry, Butterworth Heinemann Publishers.

[27] Schiewer, S. and Volesky, B., (1995) Mathematical evaluation of the experimental and modeling errors in biosorption, Biotechnology Techniques,vol. 9, No. 11, pp.845-848

[28] Dutta, P., and Beshok, A., (2001) Analytical solution of combined Electro-osmotic / pressure driven flows in two-dimensional straight channels: Finite Deybe layer effects, *Journal of Analytical Chemistry*, 73, 1979-19

[29] R.J. Hunter (1989) *Foundations of colloid science*, Oxford University Press

[30] LaLonde, A., Norton, M.G., Zhang, D., Gangadean, D., Alkhateeb, A., and McIlroy, D., (2006) A rapid method for growth of nanoparticles on nanowire Substrates, Journal of Nanoparticle Research, vol.8, pp.99-104.